Regulation of keratinocyte proliferation and epidermal inflammation by meprin α–mediated cleavage of dermokine

JID Open

Vasco Köhling[1,14], Florian Peters[2,14], Inez Götting[3], Emil Fries[1], Niklas Beck[1], Fred Armbrust[1], Silje Beckinger[1], Cynthia Bülck[1], Vahap Canbay[4], Inken Harder[5], Marion Mengel[6], Malina Rüffer[1], Kira Bickenbach[1], Konstantinos Kalogeropoulos[4,7,8], Michaela Schweizer[9], Marian Lewerenz[1], Neele Schumacher[1], Nathalie Jonca[10,11], Michael Haase[12], Ronald Naumann[13], Ulrich auf dem Keller[4], Christoph Becker-Pauly[1] and Sascha Rüffer[1]

Journal of Investigative Dermatology (2026) **146,** 2189–2203; doi:10.1016/j.jid.2026.01.034

Dysregulations within the epidermal proteolytic network can cause hyperproliferative and inflammatory disorders. Although the metalloprotease meprin α is localized in the stratum basale in healthy skin, increased levels are found in the upper epidermal layers in wound healing and psoriatic lesions. To investigate a link between meprin α expression and keratinocyte proliferation, we developed a mouse model for inducible expression of pathological meprin α levels (ie, K5Mα mice). K5Mα mice developed a skin phenotype characterized by hyperkeratosis, acanthosis, parakeratosis, and barrier defect. Keratinocyte hyperproliferation and local inflammation were induced upon induction of meprin α expression. By N-terminomics, we identified dermokine, a regulator of keratinocyte proliferation and epidermal immune response, as a putative substrate of meprin α. We validated the proteolysis and identified the cleavage site, which is highly conserved in mammals, suggesting that dermokine degradation by meprin α represents a central mechanism in wound healing and hyperproliferative skin diseases.

Keywords: Hyperproliferation, Ichthyosis, Inflammation, Meprin alpha, N-Terminomics, Proteolysis

INTRODUCTION

Epidermal homeostasis and barrier function is regulated by a complex proteolytic network that controls keratinocyte proliferation and differentiation. Proteases process proteins that form the cornified envelope and regulate the proliferation and differentiation of keratinocytes by the release and degradation of growth factors as well as cleavage of cell–cell and cell–matrix interactions (de Veer et al, 2014; Ovaere et al, 2009; Sotiropoulou et al, 2022). The expression of proteases in the epidermis is regulated by the differentiation status of keratinocytes, and their activity is controlled by protease inhibitors as well as other proteases within the network. Thereby, it is ensured that the activity of each protease is restricted to distinct layers of the epidermis (de Veer et al, 2014). Mislocalizations and dysregulated protease activities can cause defects in keratinocyte differentiation, which in turn lead to loss of barrier integrity, keratinocyte hyperproliferation, and/or inflammatory responses (Chavanas et al, 2000; Kishibe, 2019; Komatsu et al, 2007; Morizane et al, 2022). The metalloproteases meprin α and meprin β are part of the epidermal protease network. Although both exhibit similar cleavage specificities with a preference for negatively charged amino acids in P1, P1′, and P2′ position, there are major differences in the synthesis, regulation, and localization of meprins (Becker-Pauly et al, 2011; Becker et al, 2003; Hahn et al, 2003; Herzog et al, 2014; Jäckle et al, 2015; Marchand et al, 1995; Ohler et al, 2010; Rösmann et al, 2002; Werny et al, 2023; Wichert et al, 2017). Whereas meprin β expression is restricted to the stratum granulosum, meprin α is synthesized in the stratum basale (Becker-Pauly et al, 2007; Kruppa et al, 2021). Recently, we showed that meprin β regulates terminal keratinocyte differentiation by shedding of the proteoglycan

[1]Biochemical Institute, Christian-Albrechts-University of Kiel, Kiel, Germany; [2]Department of Clinical Research, University of Basel, Basel, Switzerland; [3]Institute for Pharmacology and Toxicology, Freie Universität Berlin, Berlin, Germany; [4]Department of Biotechnology and Biomedicine, Technical University of Denmark, Kongens Lyngby, Denmark; [5]Department of Dermatology, Venereology and Allergology, University Medical Center Schleswig-Holstein, Kiel, Germany; [6]Department of Clinical Chemistry and Laboratory Medicine, University Medical Center Eppendorf, Hamburg, Germany; [7]Department of Bionanoscience, Delft University of Technology, Delft, The Netherlands; [8]Kavli Institute of Nanoscience, Delft University of Technology, Delft, The Netherlands; [9]Center for Molecular Neurobiology, University Medical Center Eppendorf, Hamburg, Germany; [10]Toulouse Institute for Infectious and Inflammatory Diseases (Infinity), University of Toulouse, French National Center for Scientific Research (CNRS), French National Institute of Health and Medical Research (INSERM), Toulouse University, Toulouse, France; [11]Department of Cell Biology and Cytology, Federative Institute of Biology, Purpan University Hospital, Toulouse, France; [12]Department of Pediatric Surgery, Faculty of Medicine and University Hospital Carl Gustav Carus, TU Dresden, Dresden, Germany; and [13]Transgenic Core Facility, Max Planck Institute for Molecular Cell Biology and Genetics, Dresden, Germany

[14]These authors contributed equally to this work.

Correspondence: Sascha Rüffer, Biochemical Institute, Christian-Albrechts-University of Kiel, Otto-Hahn-Platz 9, Kiel 24118, Germany. E-mail: srueffer@biochem.uni-kiel.de and Christoph Becker-Pauly, Biochemical Institute, Christian-Albrechts-University of Kiel, Otto-Hahn-Platz 9, Kiel 24118, Germany. E-mail: cbeckerpauly@biochem.uni-kiel.de

Abbreviations: CTF, C-terminal fragment; TAILS, Terminal amine isotopic labeling of substrates; TAM, 4-hydroxytamoxifen; WT, wild-type

Received 2 October 2025; revised 15 January 2026; accepted 26 January 2026; accepted manuscript published online 10 February 2026; corrected proof published online 11 March 2026

syndecan-1 and melanogenesis by activation of IL-18 in mice (Peters and Rahn et al, 2021). So far, the epidermal role and degradome of meprin α is poorly characterized. The only evidence toward the epidermal function of meprin α arises from few in vitro data as well as its levels and localization in healthy skin compared with those in psoriatic lesions, in which increased meprin α levels have been found mislocalized to the stratum spinosum (Becker-Pauly et al, 2007). Therefore, we asked whether dysregulated meprin α activity can be causative for the onset or progression of hyperproliferative and/or inflammatory skin disorders.

To address these questions, we developed a transgenic mouse model that allows epidermis-specific induction of meprin α overexpression, thereby mimicking increased meprin α levels as observed in psoriasis vulgaris. Our aim was to characterize the skin phenotype of these mice and identify new epidermal substrates of meprin α by N-terminomics.

RESULTS

K5Mα mice develop a severe ichthyosis throughout the body upon induction of meprin α overexpression

K5Mα mice were generated by insertion of a construct comprising the C-terminal hemagglutinin-tagged murine meprin α cDNA sequence with an upstream stop cassette flanked by loxP sites and a CAG promotor into the Rosa26 locus of C57BL/6J mice. These mice were crossed with a driver strain that harbors the information for the CreER^{T2} fusion protein downstream of the keratin 5 promoter, which is highly active in keratinocytes of the stratum basale. Respective control mice did not express CreER^{T2} but harbored the transgenic Rosa26 locus (Figure 1a). For induction of CreER^{T2} translocation in mice aged 8–12 weeks, tamoxifen was applied by supplemented food pellets. Within the first week, we noticed a mild phenotype characterized by slight reddening of the ears as well as small scabby lesions around the muzzle and in the neck accompanied by occasional scratching behavior (Figure 1b, left). In the following days, we observed development of a moderate phenotype severity characterized by strong redness of the ears with prominent scabby lesions, a swollen scabby muzzle, and scabby red lesions developing over the whole body, including the extremities (Figure 1b, middle). The terminal strong phenotype was characterized by intense redness and scaling as well as skin stiffening. We also noted very frequent scratching indicating severe itching, leading to hair loss and wounding in respective skin areas (Figure 1b, right). Of note, control mice developed none of the described phenotypic changes over the whole experimental course. Between day 14 and 16, K5Mα mice developed the strong skin phenotype, which was accompanied with a very bad overall condition. Owing to large open wounds, severe hypomotility, signs of severe pain, as well as a rapid and drastic decrease of both body weight and temperature (data not shown), we had to remove all mice from the experiment latest by day 17. Three of 22 K5Mα mice even unexpectedly died before day 17. On the basis of our observations, we developed a cumulative scoring system to rate and track the skin phenotype development (Materials and Methods). Correlation analyses highlighted an exponential amplification of the skin phenotype severity with a maximum score of 20 reached within 17 days (Figure 1c). Histological examinations revealed a prominent ichthyosis in the skin of K5Mα mice (Figure 1d) accompanied by significantly higher meprin α activity than in control mice (Figure 1e).

K5Mα mice develop hyperkeratosis, acanthosis, and parakeratosis accompanied by barrier integrity defects

To characterize the progression of ichthyosis development in a defined skin area of K5Mα mice longitudinally more precisely, we treated shaved skin areas at the flank by a single local, cutaneous application of 4-hydroxytamoxifen (TAM) and sampled respective skin areas daily from killed mice over a time course of 6 days. Although no histological changes were observed in the skin of control mice, hyperplastic epidermal lesions were found in K5Mα mice already on day 2 after TAM treatment (Figure 2a). Thickness of the epidermis from K5Mα but not control mice significantly increased over the experimental period (Figure 2b), whereas dermal thickness was not altered in both K5Mα and control mice (Figure 2c). Indicative for an epidermal barrier defect, we detected an increasing transepidermal water loss on the skin areas of K5Mα but not control mice (Figure 2d). Besides the prominent hyperkeratosis, parakeratosis, and acanthosis (Figure 2e, K5Mα [I]), we identified strongly granulated keratinocytes within the stratum spinosum (Figure 2e, K5Mα [II]) and found evidence for proliferating keratinocytes in the stratum spinosum of K5Mα mice (Figure 2e, K5Mα [III] + [IV]). In addition, we observed an accumulation of lipid droplets in the stratum corneum of K5Mα mice (Figure 2f). Hemidesmosomes, lamina lucida, and lamina densa were detectable in both the skin of control mice and lesional skin areas in K5Mα mice 6 days after tamoxifen treatment, indicating an intact basement membrane (Figure 2g and h).

Keratinocyte hyperproliferation in the skin of K5Mα mice

The rapidly increasing epidermal thickness indicated keratinocyte hyperproliferation as a driving mechanism for development of the skin phenotype in K5Mα mice. Because we hypothesized that meprin α regulates keratinocyte proliferation, we assessed meprin α levels and activity as well as Ki-67 status in the skin (Figure 3a). In skin sections of control mice, we detected low but constant meprin α levels, whereas increasing and significantly higher protein levels (Figure 3b) and activity (Figure 3c) were detected in the skin of K5Mα mice. The proportion of Ki-67–positive keratinocytes in the skin of K5Mα mice significantly increased from day 1 to 6 (Figure 3d). On day 6, Ki-67 was detectable in the nuclei of over 30% of the keratinocytes in the skin of K5Mα mice. Of note, Ki-67–positive keratinocytes were also found in the stratum spinosum, and meprin α levels significantly correlated with the proportion of Ki-67–positive keratinocytes (Figure 3e). To characterize changes in the skin proteome that come with the hyperproliferative skin phenotype in K5Mα mice, we performed proteomics on skin samples (Supplementary Figure S1a). On day 3 after TAM treatment, we detected massive changes in the skin proteome of K5Mα (Supplementary Figure S1b–d and Supplementary Data). In line with our histological findings, we found higher and increasing levels of proteins associated with the formation of the cornified envelope. Most prominently, we detected significantly higher levels of keratins 16 and 6b as well as

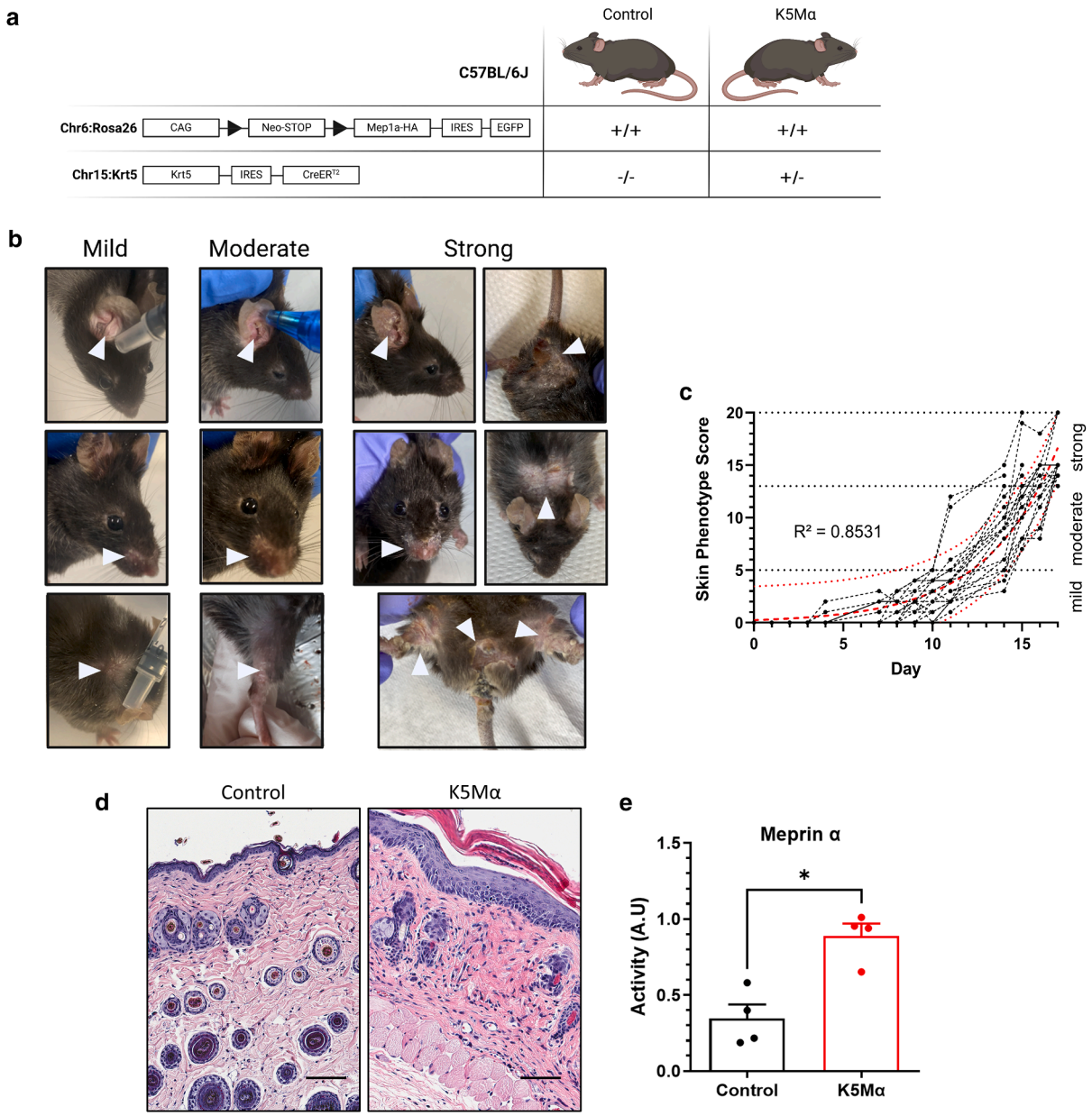

Figure 1. K5Mα mice develop a severe ichthyosis throughout the body upon induction of meprin α overexpression. **(a)** Control and K5Mα mice were bred on a C57BL7/6J background harboring a homozygous (+/+) insertion in the Rosa26 locus composed of a CAG-promotor (CAG), a loxP site (►)-flanked neomycin resistance (Neo)/STOP cassette, a cDNA sequence encoding HA-tagged murine meprin α (*Mep1a*-HA), an IRES, and a cDNA sequence encoding *EGFP*. K5Mα mice carry heterozygous (+/−) downstream of the *K5* gene an IRES followed by a gene encoding the fusion protein CreER^{T2}. **(b)** Development of the skin phenotype in K5Mα mice after start of the tamoxifen treatment. Representative images of the macroscopic skin examination are shown. White arrowheads mark the examined skin area. **(c)** Cumulative skin phenotype scores calculated from macroscopic skin examination of K5Mα mice (n = 22) from day 0 to day 17 after start of tamoxifen treatment. R-square (R^2) value was calculated by nonlinear regression on the basis of an exponential growth equation. **(d)** Representative microscopical images of H&E-stained skin sections from control and K5Mα mice after 17 days of tamoxifen treatment. Bar = 75 μm. **(e)** Meprin α activity in skin lysates of control (n = 4) and K5Mα (n = 4) mice after 17 days of tamoxifen treatment. Activity is plotted in A.U. Bar charts and error bars display mean ± SEM. Statistically significant differences ($P < .05$) are labeled by an asterisk (*). Graphical illustration in **a** was created with BioRender.com. A.U., arbitrary unit; HA, hemagglutinin; IRES, internal ribosomal entry site.

markedly higher levels of keratin 6a in the skin of K5Mα mice (Supplementary Figure S1e and f).

In summary, our analyses showed that the onset of the skin phenotype takes place already within the first 3 days after TAM treatment. Therefore, we focused our following analyses on this time period.

Local inflammatory response in the skin of K5Mα mice

In K5Mα skin sections, we noticed a strong infiltration of immune cells (Figure 4a) and observed prominently enlarged vessels, both indicative for an inflammatory response (Figure 4b). Detection of meprin α and CD45 validated a strong infiltration of leukocytes, particularly in areas with

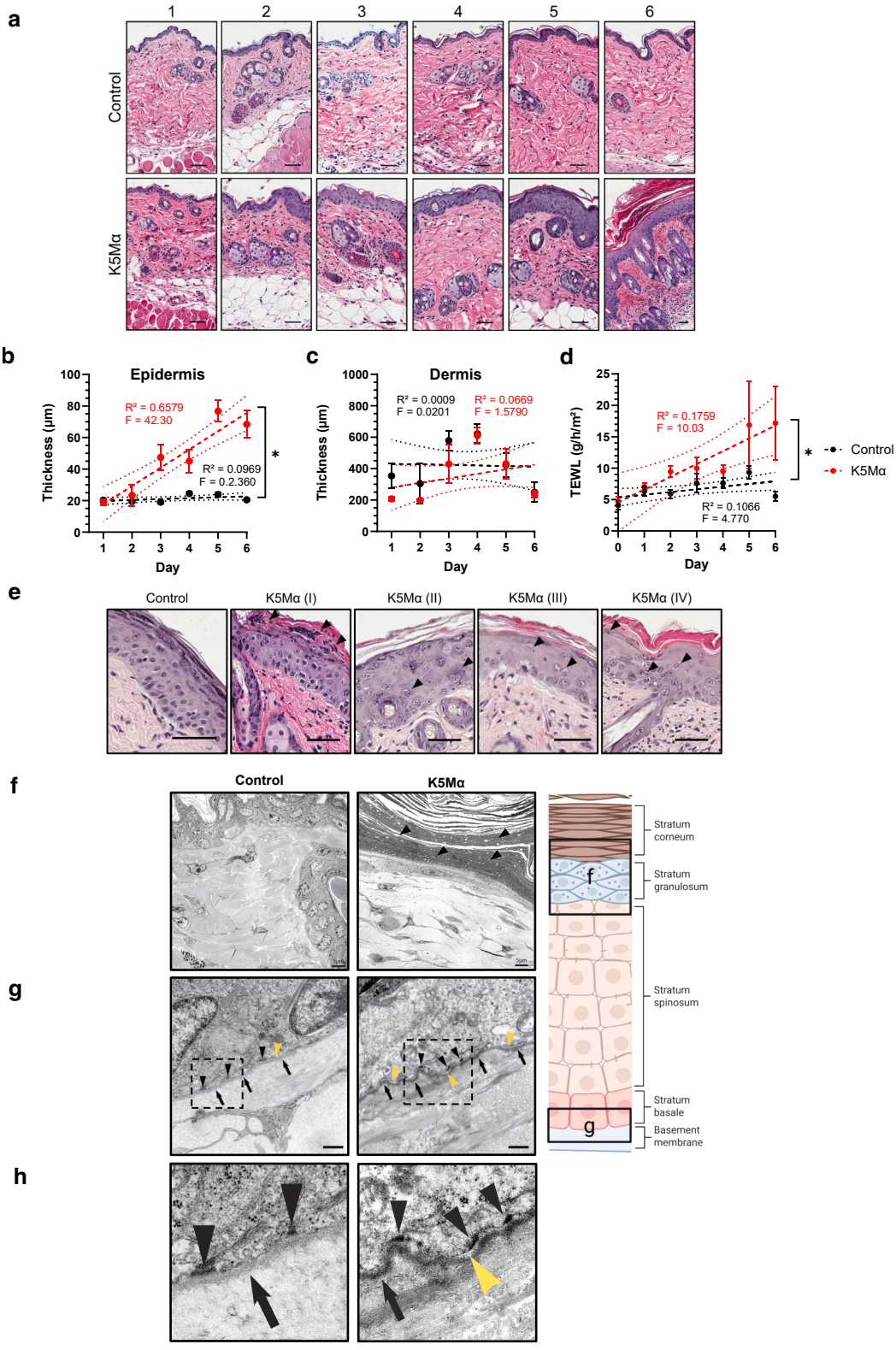

Figure 2. K5Mα mice develop hyperkeratosis, acanthosis, and parakeratosis accompanied by a loss of barrier integrity. **(a)** H&E-stained skin sections from control (n = 8 per day) and K5Mα (n = 8 per day) mice. Bar = 67 µm. **(b)** Epidermal thickness of control (n = 4 per day) and K5Mα (n = 4 per day) mice. Data are provided as mean ± SEM. Slopes were tested for significant difference (2-tailed *t*-test, $P < .0001$). **(c)** Dermal thickness of control (n = 4 per day) and K5Mα (n = 4 per day) mice. Data are provided as mean ± SEM. Slopes were tested for significant difference (2-tailed *t*-test, $P = .3392$). **(d)** TEWL through skin areas of control (n = 5) and K5Mα (n = 6) mice. Data are provided as mean ± SEM. Slopes were tested for significant difference (2-tailed *t*-test, $P = .0279$). **(b–d)** Simple linear regression (dashed lines) and respective 95% confidence band of the best-fit line (dotted lines) are displayed. **(e)** H&E-stained skin sections from control and K5Mα mice. Arrowheads mark hyperkeratotic and parakeratotic lesions (K5Mα (I)), highly granulated keratinocytes in the spinous layer accompanied by acanthosis (K5Mα (II)), as well as suprabasal proliferating keratinocytes (K5Mα (III + IV)). Bar = 50 µm. **(f, g)** Transmission electron microscope images of skin sections from control and K5Mα mice with a focus on **(f)** the upper spinous layer, stratum granulosum, and stratum corneum or **(g)** the basal layer and the

high epidermal meprin α levels (Figure 4c). In our proteomics data, we identified higher levels of CD45, CD11b, and Ly6c (Figure 4d) as well as neutrophilic granulocyte-specific effector and regulator proteins (Figure 4e) in the skin of K5Mα mice. High S100A9 levels were detected in infiltrating leukocytes as well as keratinocytes (Figure 4f). Expression of *S100a9* and *S100a8* was significantly higher in the skin of K5Mα than in that of control mice (Figure 4g). Moreover, we observed increasing and significantly higher levels of IL-6, IL-17A, and TNFα as well as GM-CSF, CXCL1, and CCL2 in the skin of K5Mα than in that of control mice (Figure 4h). In addition, we validated significantly increasing expression of *Il1b*, *Il6*, *Il17a*, *Il36g*, *Tnfa*, *Saa1*, *Csf2*, *Csf3*, *Cxcl1*, and *Ccl2* in the skin of K5Mα (Supplementary Figure S2).

Identification of potential epidermal meprin α substrates by N-terminomics

For identification of potential meprin α substrates that cause phenotype development in K5Mα mice, we performed terminal amine isotopic labeling of substrates (TAILS) (Figure 5a), an N-terminomics approach that enables the detection proteolytically generated neo-N-termini, and applied a stepwise filtering for meprin α–specific cleavage criteria (Supplementary Figure S3 [details are provided in Materials and Methods). In total, we detected 41,619 peptides in the skin of K5Mα and control mice. Of note, we did not detect any peptide with our settings that was exclusively present in the dataset of either control or K5Mα mice, indicating that all identified peptides in the skin of K5Mα mice were also generated physiologically. Thereby, we identified 6 peptide candidates on day 1, 10 peptide candidates on day 2, and 10 peptide candidates on day 3, which were derived from 10 different proteins in total (Supplementary Figure S3, Figure 5b, and Table 1). Normalization of the candidate peptide levels to their respective total protein levels revealed that only the dermokine-derived peptide was significantly higher abundant in the skin of K5Mα mice already on day 1 (Figure 5c). Modeling each substrate candidate in complex with either the monomeric or homodimeric meprin α ectodomain with AlphaFold 3 (Abramson et al, 2024), we identified a model of homodimeric meprin α in complex with dermokine that would result in cleavage of dermokine between F297 and D298 (Supplementary Figure S4a) as well as between R439 and A440 (Supplementary Figure S4b), cleavage events that both would result in peptides detected by TAILS. Therefore, we focused our further analyses on dermokine as a potential epidermal meprin α substrate.

Validation of dermokine as a meprin α substrate

In total, we identified 14 different peptides derived from dermokine isoforms (Figure 6a). Thirteen of the identified peptides were covered by isoform 1 (dermokine β) and isoform 4. Eleven peptides were covered by isoform 2 (dermokine γ) and isoform 1. Only 1 peptide (H_{22}SWGSDLSSLQKR) was exclusively covered by isoform 3 (dermokine α), a truncated isoform of about 11.5 kDa. Indicative for an elevated dermokine turnover, we detected 5 dermokine-derived peptides that were significantly higher abundant and 3 more peptides that were almost 1.5-fold higher abundant in the skin of K5Mα than in control mice already on day 1 (Figure 6a). To test whether meprin α can cleave dermokine, we transfected human embryonic kidney 293T cells with plasmids encoding wild-type (WT) *Mep1a*, C-terminal Myc-FLAG-tagged *Dmkn*, and a catalytically inactive *Mep1a* variant (E155A) (Supplementary Figure S4c). The *Dmkn* sequence encoding dermokine β (UniProt identification: Q6P253-4) comprised all putative cleavage sites identified by TAILS except for the one that was exclusively present in dermokine α. Western blot analyses revealed a prominent C-terminal fragment (CTF) of dermokine with a size of about 45 kDa exclusively present under coexpression of *Mep1a* WT and *Dmkn* (Figure 6b). In line, we observed lower levels of full-length dermokine (~55 kDa) in these lysates (Figure 6c). Interestingly, we detected significantly higher levels of full-length dermokine under coexpression of *Mep1a* E155A and *Dmkn* (Figure 6c), indicating a potential stabilizing non-proteolytical interaction. Indeed, we validated the interaction of both meprin α WT and meprin α E155A with dermokine by coimmunoprecipitation after pull down of dermokine (Figure 6d) as well as meprin α (Figure 6e). Notably, we also detected the putative meprin α–generated dermokine CTF after pull down of meprin α, supporting that this CTF is directly generated by meprin α and not by other proteases, which might be activated directly or indirectly by meprin α (Figure 6e).

To identify the cleavage site that leads to formation of this dermokine CTF, we performed a proteomics analysis after coimmunoprecipitation of dermokine from lysates of human embryonic kidney 293T cells transfected with the plasmid encoding *Dmkn* alone or in combination with either *Mep1a* WT or *Mep1a* E155A. Validating the interaction of dermokine and meprin α, we identified both dermokine and meprin α among the highest abundant proteins in the coimmunoprecipitates (Supplementary Figure S4d). In total, we detected 86 dermokine-derived peptides covering 72% of its total sequence. Among these 86 peptides, we identified 20 peptides higher abundant (≥1.5-fold) in the immunoprecipitates after coexpression of *Mep1a* WT and *Dmkn* than after expression of *Dmkn* alone (Supplementary Figure S4e). Among these 20 peptides, 12 peptides harbored a tryptic cleavage site (Supplementary Figure S4e, red marked), and 2 peptides were likely derived by canonical release of the N-terminal signal peptide. Within the remaining 6 peptides, only 3 were identified that could correspond to a CTF with a size of about 45 kDa (Supplementary Figure S4e). In this study, we identified significantly higher levels of [G].E_{93}AARSLGNAGNEIGR in the immunoprecipitates after coexpression of *Mep1a* WT and *Dmkn* (Figure 6f) but not after coexpression of catalytically inactive *Mep1a* E155A and *Dmkn* (Figure 6g). Therefore, our data suggest that meprin α cleaves dermokine between G92 and E93, a cleavage site that fits very well to the cleavage preference of meprin α. Detection of dermokine and meprin α in skin sections of

basement membrane. **(f)** Arrowheads mark lipid droplets in the stratum corneum. Bars = 5 μm. **(g)** Black arrowheads mark hemidesmosomes, yellow arrowheads mark the lamina lucida, and black arrows mark the lamina densa. Bars = 500 nm. **(h)** Magnification of the area marked in **g** with a focus on hemidesmosomes. Graphical illustrations in **f** and **g** were created with BioRender.com. Statistically significant differences ($P < .05$) are labeled by an asterisk (*). TEWL, transepidermal water loss.

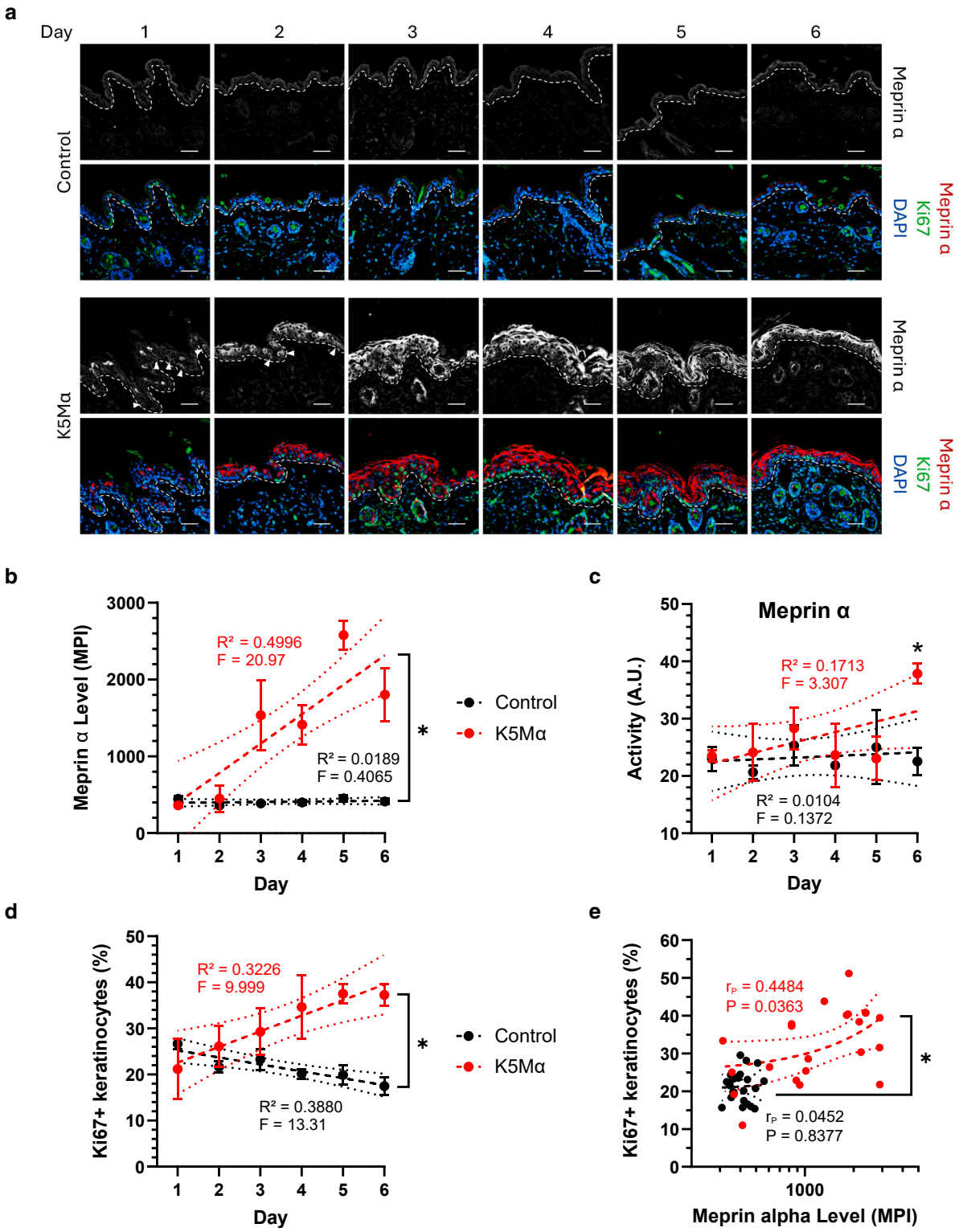

Figure 3. Keratinocyte hyperproliferation correlates with meprin α levels in K5Mα mice. **(a)** Meprin α (red) and Ki-67 (green) in skin sections from control (n = 4 per day) and K5Mα (n = 4 per day) mice. Nuclei were stained with DAPI. Bars = 50 μm. **(b)** MPI from meprin α staining in skin sections from control (n = 4 per day) and K5Mα (n = 4 per day) mice. Data are presented as mean ± SEM. Simple linear regression (dashed lines) and respective 95% confidence band of the best-fit line (dotted lines) are displayed. Slopes were tested for significant difference (2-tailed *t*-test, $P > .0001$). **(c)** Meprin α activity in skin lysates of control (n = 4 per day) and K5Mα (n = 4 per day) mice. Activity is plotted in A.U. Data are presented as mean ± SEM. Simple linear regression (dashed lines) and respective 95% confidence band of the best-fit line (dotted lines) are displayed. Slopes were tested for significant difference (2-tailed *t*-test, $P = .2670$). **(d)** Proportion of Ki-67–positive keratinocytes in skin sections from control (n = 4 per day) and K5Mα (n = 4 per day) mice. Data are provided as mean ± SEM. Simple linear regression (dashed lines) and respective 95% confidence band of the best-fit line (dotted lines) are displayed. Slopes were tested for significant difference (2-tailed *t*-test, $P = .0001$). **(e)** Correlation of meprin α levels and Ki-67 status in skin sections from control (n = 23) and K5Mα (n = 23) mice. Simple linear regression (dashed lines) and respective 95% confidence band of the best-fit line (dotted lines) are displayed for control ($R^2 = 0.002043$, F = 0.04299) and

control and K5Mα mice (Figure 6h) revealed significantly lower and decreasing dermokine levels in the skin of K5Mα mice (Figure 6i), whereas *Dmkn* mRNA levels were not altered (Supplementary Figure S4f). Moreover, our analyses showed that increasing meprin α levels correlated with a decreasing dermokine colocalization (Figure 6j), and particularly hyperplastic epidermal areas were characterized by high meprin α levels (Figure 6j). Supporting our hypothesis that dermokine cleavage by meprin α initiates phenotype onset in K5Mα mice by decreasing the amount of functional dermokine, our proteomics data revealed markedly lower ($P = .0683$) dermokine levels in K5Mα mice on day 1 after induction of meprin α overexpression (Supplementary Figure S4g). Speculating about potential functional consequences of dermokine cleavage by meprin α at the identified site, we modeled the structure of dermokine using AlphaFold 3 (Supplementary Figure S4h). AlphaFold 3 calculated very low (pIDDT < 50) and low (70 > pIDDT > 50) prediction scores as well as a very low predicted template modeling score of only about 0.2 for most of the models. The highest prediction scores were calculated for a sequence of 104 amino acids ranging from N22 to S125, which was reproducibly predicted to fold into 2 alpha helices, with the meprin α cleavage site located in the N-terminal alpha helix of this sequence (Supplementary Figure S4h). Finally, we aligned the dermokine sequence around the identified meprin α cleavage site from various mammals. Strikingly, our analysis indicated that this region is highly conserved in mammals (Supplementary Figure S4i). Supporting our hypothesis that meprin α acts as a conserved regulator of dermokine in mammals, we identified rapidly decreasing levels of human dermokine upon incubation with active recombinant human meprin α (Supplementary Figure S4j).

DISCUSSION

Dermokine was identified and first described in 2004 by Matsui et al (2004) as a protein secreted by differentiating keratinocytes in the spinous layer of murine and human epidermis. For murine dermokine, there are 3 major secreted isoforms annotated, namely α, β, and γ (Leclerc et al, 2014). For *Dmkn* βγ-deficient mice, a transient scaly skin phenotype that disappeared 1 week after birth has been reported (Leclerc et al, 2014; Utsunomiya et al, 2020). In contrast, *Dmkn* αβγ-deficient mice developed a progressively increasing severe ichthyosis (Utsunomiya et al, 2020). On the basis of its negative regulatory effects on extracellular signal–regulated kinase signaling (Higashi et al, 2012), dermokine was proposed as a negative regulator of keratinocyte proliferation that balances the differentiation status of keratinocytes (Utsunomiya et al, 2020). Although there is increasing evidence that dermokine acts on various intracellular signaling cascades (Canbay et al, 2025[1]; Hasegawa et al, 2013a; Higashi et al, 2012), its regulation and the molecular mode of action are so far unknown. Because meprin α overexpression in K5Mα mice causes a loss of epidermal dermokine, and the ichthyosis observed in K5Mα mice represents a striking phenocopy of *Dmkn* αβγ-deficient mice, we propose that cleavage by meprin α causes the functional inactivation of dermokine.

Our data strongly support that initiation of the skin phenotype in K5Mα mice is triggered by keratinocyte hyperproliferation. Besides the changes observed in Ki-67 status, our proteomics data revealed increasing levels of the proliferating cell nuclear antigen (Kawahira, 1999) and 15 other proteins associated with regulation of the cell cycle and proliferation. Moreover, our histological analyses indicated that keratinocyte hyperproliferation also takes place in suprabasal layers of the epidermis, which has already been reported in the context of wound re-epithelialization (Usui et al, 2005) and psoriasis vulgaris (Kim et al, 2018). In addition, we observed highly increased levels of keratins 6a, 6b, and 16 in the skin of K5Mα mice, a characteristic event for keratinocytes that acquire a highly proliferative phenotype, because these keratins are almost absent in keratinocytes of the interfollicular epidermis under homeostatic conditions (McGowan and Coulombe, 1998; Zhang et al, 2019).

Supporting a mechanistic link between meprin α, dermokine, and keratinocyte proliferation, meprin α is highly abundant in epidermal tongues during wound re-epithelialization (Kruppa et al, 2021). In addition, increased dermokine expression has been reported in epidermal tongues during early stages of wound healing in mice (Leclerc et al, 2014). However, having a closer look at the immunostainings of dermokine in this publication, we noted rather a lower staining intensity particularly at the wound edges than at distal epidermal areas. In line, it has been reported that particularly early wound healing is significantly delayed by topical treatment with recombinant dermokine β (Hasegawa et al, 2013a). In psoriatic lesions, meprin α is highly abundant and relocated to suprabasal layers (Becker-Pauly et al, 2007). The same localization was reported for dermokine in psoriasis vulgaris (Hasegawa et al, 2013b). In this study again, dermokine staining intensity in the representative psoriatic lesions appeared markedly lower to us than representative sections from other skin pathologies. These observations match with our findings that epidermal dermokine levels are drastically reduced upon meprin α overexpression, and the absence of dermokine in epidermal areas with high meprin α levels was particularly observed in hyperplastic lesions. However, it has to be further investigated whether these spatial correlations between meprin α and dermokine are due to dermokine cleavage by meprin α. In case of the mechanistic validation, this would implicate

K5Mα ($R^2 = 0.2011$, $F = 5.034$) mice. Elevations were tested for significant difference (2-tailed *t*-test, $P = .0405$). Pearson correlation and respective 2-tailed *P*-values are annotated. Statistically significant differences ($P < .05$) are labeled by an asterisk (*). A.U., arbitrary unit; MPI, mean pixel intensity.

[1] Canbay V, Wüstemann T, Tian W, Beyer TA, Elbæk CR, Stumpe M, et al. Multi-omics analysis of keratinocytes reveals dermokine-dependent regulation of cell-cell adhesion via p120. bioRxiv 2025.

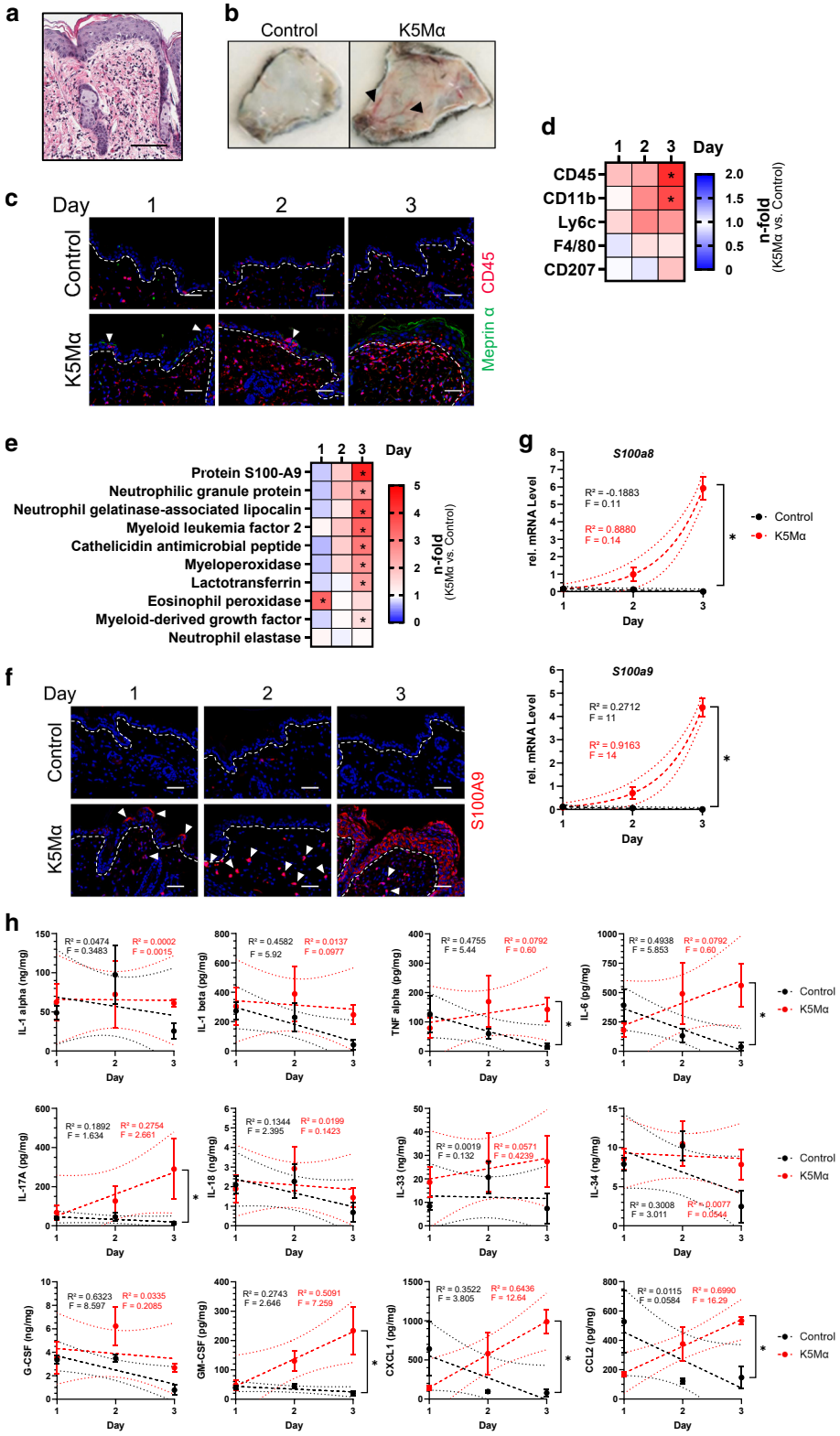

Figure 4. Local inflammatory response in the skin of K5Mα mice. **(a)** Immune cell infiltrates in the skin of a K5Mα mouse (Bar = 100 μm) as well as **(b)** photos from the dermal side of the skin from a control and K5Mα mouse. Arrowheads (◄) mark enlarged vessels. **(c)** Meprin α (green) and CD45 (red) in skin sections from control (n = 3 per day) and K5Mα (n = 3 per day) mice. Nuclei were stained with DAPI. Bars = 50 μm. **(d)** Mean n-fold changes in the levels of leukocyte lineage marker proteins detected by LC-MS/MS in the skin of K5Mα mice (n = 3 per day) compared with that of control mice (n = 3 per day). Statistical significance ($P < .05$) was tested by 2-tailed unpaired *t*-test prior to normalization. **(e)** Mean n-fold changes in the levels of leukocyte-associated effector proteins detected by LC-MS/MS in the skin of K5Mα mice (n = 3 per day) compared with that of control mice (n = 3 per day). Statistical significance ($P < .05$) was tested by 2-tailed unpaired *t*-test prior to normalization. **(f)** S100A9 (red) in skin sections from control (n = 3 per day) and K5Mα (n = 3 per day) mice. Nuclei were stained with DAPI. Bars = 50 μm. **(g)** Relative mRNA levels of *S100a8* and *S100a9* in skin samples from control (n = 5 per day) and K5Mα (n = 5 per day) mice normalized to *Gapdh* levels. Data are provided as mean ± SEM. Nonlinear regression based on an exponential growth equation (dashed lines) as well as

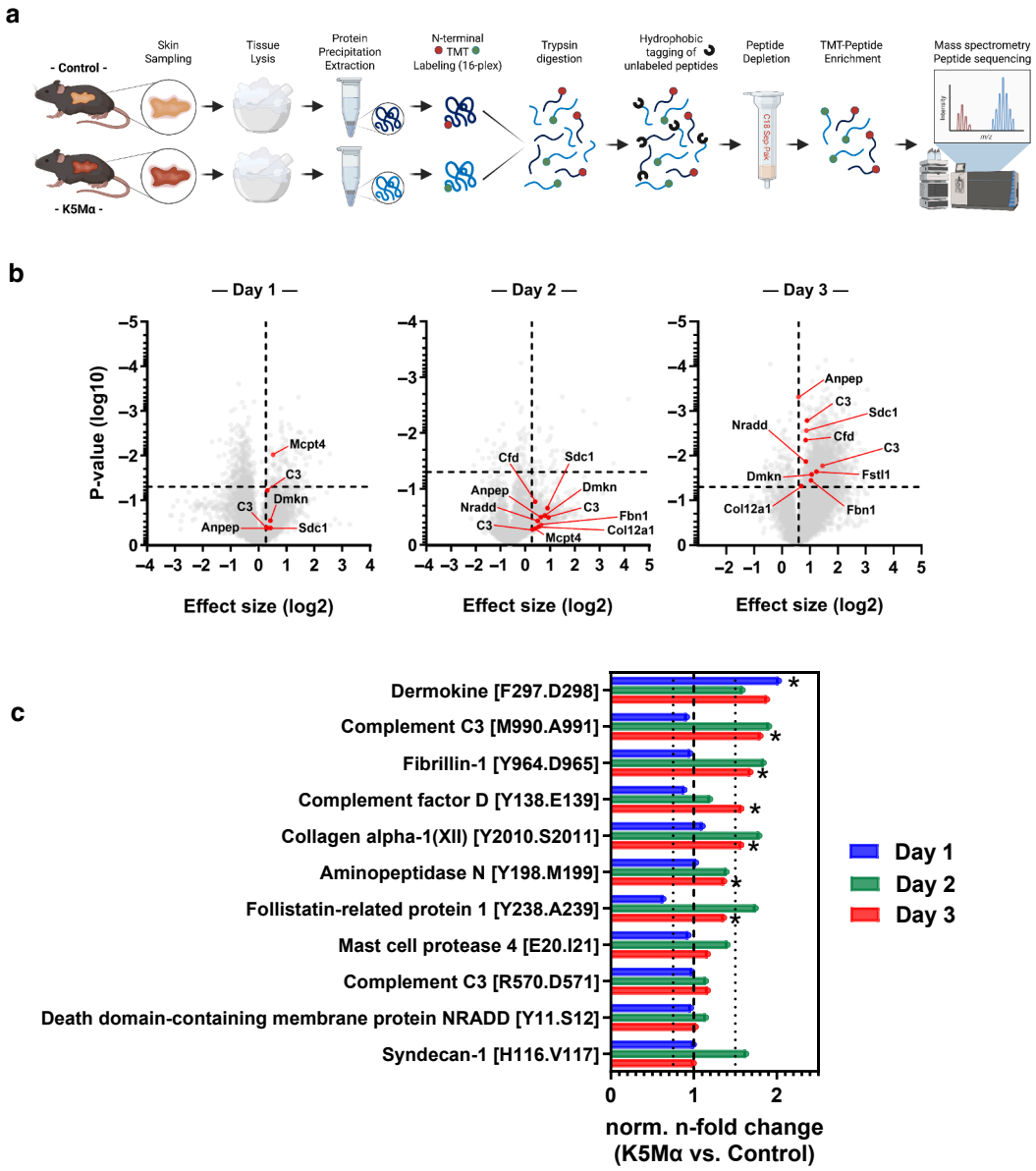

Figure 5. Identification of potential substrates by filtering N-terminomics data for meprin α–specific cleavage criteria. **(a)** Schematic illustration of the sample preparation work flow for TAILS analysis. Skin samples from control (n = 3) and K5Mα (n = 3) mice were excised after killing on days 1–6 after topical TAM treatment and pulverized in a liquid nitrogen-cooled mortar, and proteins were isolated by methanol/chloroform precipitation. Proteins were TMT labeled and trypsin digested. Peptides with neo-N termini generated by trypsin digestion were undecanal labeled and depleted by a C18 Sep-Pak column, and enriched TMT-labeled peptides were subjected to LC-MS/MS analysis. **(b)** Volcano plots display potential meprin α substrates (red dots with annotation) identified by TAILS. Dashed lines (- - -) mark thresholds for 1.2- (days 1 + 2) and 1.5-fold (day 3) changes in effect size (x-axis; log2 transformed) and a $P = .05$ (y-axis; log10 transformed); the threshold for statistical significance was assessed by 2-tailed unpaired *t*-test. All other detected peptides are depicted as gray dots. **(c)** Mean n-fold changes in the levels of peptides (annotated by corresponding proteins and putative cleavage site in squared brackets) potentially generated by meprin α on days 1 (blue), 2 (green), and 3 (red) after TAM treatment in the skin of K5Mα compared with that of control mice. Peptide levels were normalized to the total level of corresponding proteins detected by LC-MS/MS analysis. Equal levels between control and K5Mα mice (n-fold = 1) are highlighted by a dashed line (- - -), and thresholds for 0.75-fold and 1.5-fold altered levels are marked by dotted lines (• • •). Statistically significant differences ($P < .05$) between K5Mα and control mice were tested by 2-tailed unpaired *t*-test and labeled by an asterisk (*). Graphical illustration in **a** was created with BioRender.com. LC-MS/MS, liquid chromatography-tandem mass spectrometry; TAILS, terminal amine isotopic labeling of substrates; TAM, 4-hydroxytamoxifen; TMT, Tandem Mass Tag.

respective 95% confidence band of the best-fit line (dotted lines) are displayed. Curves were tested for significant differences by extra sum-of-squares F test (*S100a8*, $P < .0001$; *S100a9*, $P < .0001$). **(h)** Concentrations of cytokines and chemokines in skin lysates of control (n = 3 per day) and K5Mα (n = 3 per day) mice normalized to the respective protein concentration in the lysates. Data are provided as mean ± SEM. Simple linear regressions (dashed lines) and respective 95% confidence bands of the best-fit line (dotted lines) are displayed. Slopes (s) and elevations (e) were tested for significant differences (2-tailed *t*-test: TNFα[e], $P = .0373$; IL-6[s], $P = .0332$; IL-17A[e], $P = .0488$; GM-CSF[s], $P = .0111$; CXCL1[s], $P = .0021$; CCL2[s], $P = .0271$). Statistically significant differences ($P < .05$) are labeled by an asterisk (*). LC-MS/MS, liquid chromatography-tandem mass spectrometry.

Table 1. Putative Meprin α Substrates Identified by TAILS

Substrate Candidate	Peptide Sequence (N-C)	Peptide Score	n-Fold (*P*-Value)		
			Day 1	Day 2	Day 3
Dermokine	[**SNF**].**D_{298}EG** YSVSR.[G]	485	1.34 (.2833)	1.73 (.2973)	2.11 (.0266)
Syndecan-1	[**VLH**].**V_{117}EA** EPGFTAR.[D]	361	1.34 (.4140)	1.86 (.2187)	1.84 (.0028)
Complement C3	[**VQM**].**A_{991}ED** AVDGER.[L]	347	1.23 (.4012)	1.91 (.3217)	2.75 (.0170)
Complement C3	[**DPR**].**D_{571}NH** LAPGQQTTLR.[I]	340	1.24 (.0599)	1.22 (.5300)	1.88 (.0017)
Aminopeptidase N	[**SEY**].**M_{199}EG** DVKKVVATTQMQAADAR.[K]	303	1.24 (.4192)	1.55 (.3198)	1.51 (.0005)
Mast cell protease 4	[**AEE**].**I_{21}IG** GVESRPHSRPYMAHLEITTER.[G]	332	1.43 (.0095)	1.33 (.5087)	
Fibrillin-1	[**LKY**].**D_{965}DE** ECTLPIAGR.[H]	428		1.56 (.4398)	2.06 (.0363)
Collagen alpha-1(XII)	[**ALY**].**S_{2011}DG** EGNPSPSQGR.[T]	368		1.46 (.4766)	1.63 (.0483)
Complement factor D	[**LQY**].**E_{139}DK** EVEPGTLCDVAGWGVVTHAGR.[R]	342		1.32 (.1676)	1.81 (.0045)
Death domain-containing membrane protein NRADD	[**VVY**].**S_{12}DT** ALQGQDGDR.[E]	308		1.42 (.3720)	1.82 (.0136)
Follistatin-related protein 1	[**ETY**].**A_{239}DG** AETEVDCNR.[C]	309			2.37 (.0230)

Listed are the corresponding proteins ("Substrate Candidate"), the respective peptides detected by TAILS in 1-letter code, and the Peptide Score (sum of likelihood scores for amino acids in position P3 to P3′). Start and end of the peptide sequences are marked by a full stop. Amino acids in squared brackets are annotated on the basis of the protein sequence obtained from UniProt database. Amino acids presented in bold are located in positions P3 to P3′ to the putative cleavage site, and these amino acids were used for calculation of the Peptide Score. N-fold differences in peptide levels between K5Mα and control mice are annotated. *P*-values were calculated by 2-tailed unpaired *t*-test (n = 3 vs 3).

that (re)activation of the proliferative potential in keratinocytes is both a physiological and pathophysiological process regulated by meprin α.

Similar to *Dmkn* αβγ-deficient mice (Utsunomiya et al, 2020), our K5Mα mice developed an impaired barrier integrity characterized by an increased transepidermal water loss. In the stratum corneum of K5Mα mice, we noticed a strong accumulation of lipid droplets, a characteristic finding also reported in *Dmkn* αβγ-deficient mice (Utsunomiya et al, 2020). We assume that these lipid droplets are derived from incomplete processing of lamellar bodies in the stratum granulosum due to the excessive number of keratinocytes transitioning from the stratum granulosum into the stratum corneum. A compromised release of lipids from lamellar bodies would cause a reduced synthesis of extracellular lamellar lipid membranes and consequently lead to an impaired evaporation barrier. As indicators for an impaired stratum corneum differentiation, we observed incomplete differentiation of corneocytes and significantly higher levels of protein-glutamine gamma-glutamyl transferase 5, an enzyme that is responsible for the release and extracellular crosslinking of contents from lamellar bodies (Candi et al, 2002; De Koning et al, 2012).

Both keratinocyte hyperproliferation and epidermal barrier defects either due to wounding or skin diseases are accompanied by inflammatory responses. In this context, it has been reported that dermokine acts as a negative regulator of ELR + CXC chemokine expression (Hasegawa et al, 2013a). Supporting a functional inactivation of dermokine by meprin α, we detected highly elevated CXCL1 levels in the skin of K5Mα mice, which might initiate the subsequent inflammatory cascade. Supporting this hypothesis, there is a striking overlap between dysregulated gene expression patterns reported in *Dmkn* αβγ-deficient mice and K5Mα mice (Utsunomiya et al, 2020).

Most N-termini of the highly abundant dermokine-derived peptides identified by TAILS were located near the C-terminal globular domain 2, which has been described as the functional domain of dermokine with regard to modulation of extracellular signal−regulated kinase signaling (Hasegawa et al, 2013a; Higashi et al, 2012). Because the meprin α cleavage site between G92 and E93 is located distant to this functional domain, we assume that the initial cleavage by meprin α makes dermokine prone to additional subsequent proteolytic events executed in part either by meprin α itself or by other proteases. Supporting this hypothesis, we detected drastic alterations in the abundance of dermokine-derived peptides in the skin of K5Mα mice and upon coexpression of dermokine and meprin α in vitro. Although AlphaFold 3−based structural predictions for most of the dermokine sequence were very uncertain, the meprin α cleavage site was located in a reproducibly modeled alpha helix, which might indicate a relevance of this domain for the folding, stability, and/or signaling of dermokine. Noteworthy, meprin α cleavage of dermokine, particularly at this site, would explain why we did not detect the corresponding peptide by TAILS, because tryptic cleavage between R96 and S97 during sample preparation causes loss of the peptide comprising this neo-N-terminus ([G].E_{93}AA$R_{96}$$S_{97}$LGNAGNEIGR). Although we could not experimentally confirm the cleavage site between F297 and D298 suggested by AlphaFold 3 modeling using our in vitro system, the AlphaFold 3 models were very helpful in confirming potential interaction with dermokine. It was notable that no modeling of meprin α with any of the other identified candidates yielded a hypothetical interaction that would lead to the formation of the respective peptides. Furthermore, we cannot exclude that the cleavage site between F297 and D298 might still be utilized by meprin α in the much more complex skin system. Beyond the extracellular environment and potential differences in the expression and processing of dermokine and meprin α in keratinocytes compared with those in human embryonic kidney 293T cells, the

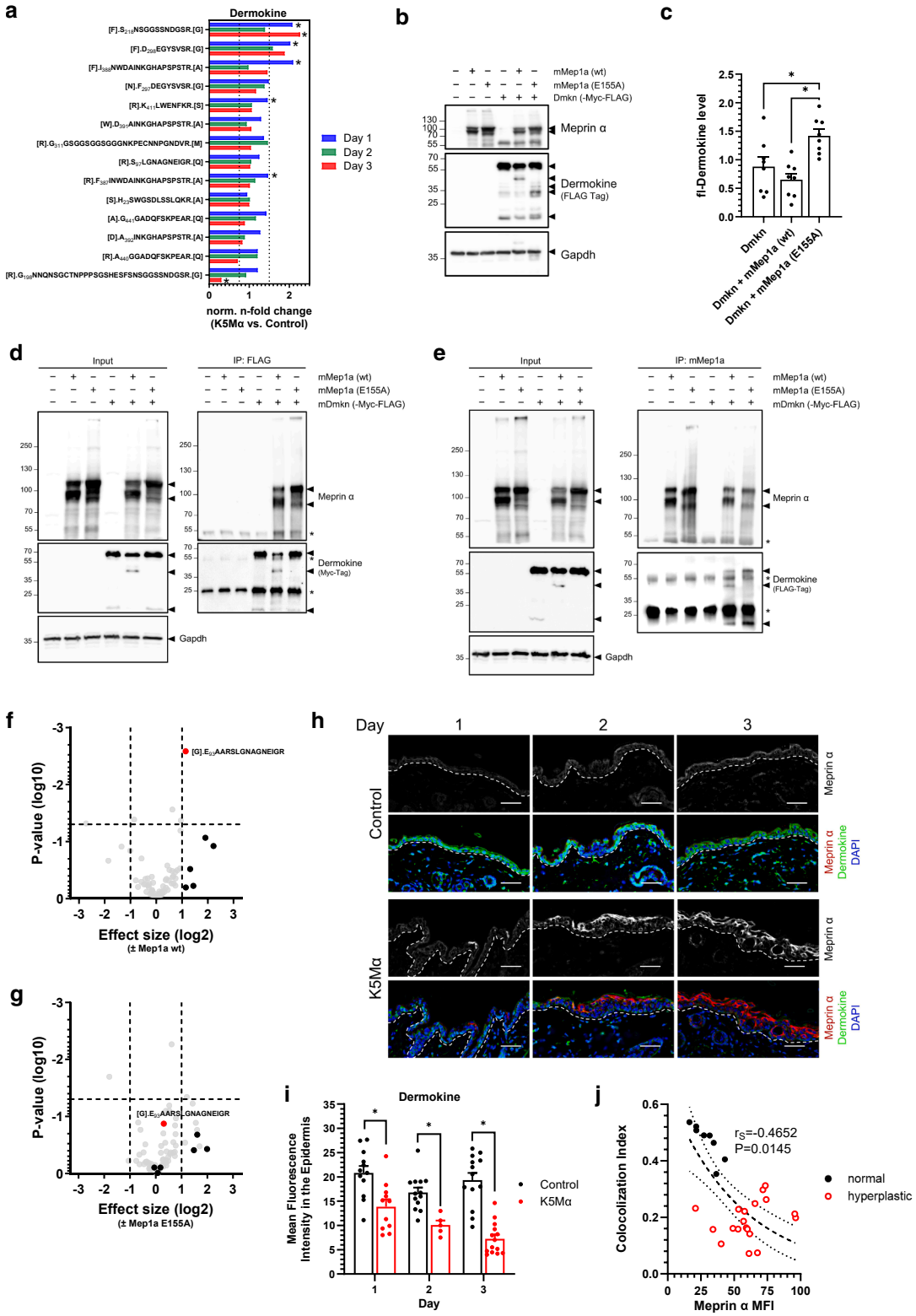

Figure 6. Validation of dermokine cleavage by meprin α. **(a)** Mean n-fold changes in the levels of dermokine-derived peptides detected by TAILS on days 1 (blue), 2 (green), and 3 (red) in the skin of K5Mα compared with that of control mice. Peptide levels were normalized to the total dermokine level detected by LC-MS/MS. Thresholds (0.75-fold and 1.5-fold) are marked by dotted line (●●●). Statistical significance (*$P < .05$) was tested by 2-tailed unpaired *t*-test. **(b)** Meprin α and dermokine in lysates of HEK293T cells transiently transfected with an empty control plasmid or plasmids encoding WT murine meprin α (*Mep1a*), C-terminally Myc-FLAG-tagged murine dermokine (*Dmkn*), and/or a catalytically inactive meprin α variant (*Mep1a* (E155A)). Gapdh was detected as a reference (n = 8). **(c)** Full-length (denoted as fl) dermokine levels (>55 kDa signal in **b**) normalized to respective Gapdh levels. Data are provided as mean ± SEM. Statistical significance (*$P < .05$) was tested by RM 1-way ANOVA ($P = .0165$) and Tukey post-test (Dmkn vs Dmkn + mMep1a [E155A]: $P = .0337$; Dmkn +mMep1a [WT] vs Dmkn + mMep1a [E155A]: $P = .0336$). **(d, e)** Meprin α and dermokine in lysates of HEK293T cells transiently transfected as indicated before (input) and after IP of **(d)** dermokine (IP:Flag) or **(e)** meprin α (IP: mMep1a). Gapdh was detected as references in input lysates. Light and heavy chains of

formation of the meprin α/meprin β heterodimer could also lead to altered cleavage (Bülck et al, 2023; Peters et al, 2019).

In summary, we propose that meprin α cleavage counteracts dermokine function and thereby indirectly regulates keratinocytes proliferation and immune cell recruitment. Moreover, available data on their epidermal localization and expression levels indicate that meprin α–mediated cleavage of dermokine represents a relevant physiological mechanism in wound healing and hyperproliferative skin diseases.

MATERIALS AND METHODS

Chemicals

All chemicals were purchased of analytical grade from Merck, Carl Roth, Thermo Fisher Scientific, or Roche.

Animal care

Animal acquisition, breeding, accommodation, care, and usage in experimental procedures were performed in accordance with the guidelines of the German National Committee for the Protection of Animals Used for Scientific Purposes. Animals were housed under specific pathogen-free conditions in an individually ventilated cage system at constant environmental conditions (12-hour light–dark cycle, 22 ± 2°C, 55 ± 10% relative humidity). A maximum of 5 male or female siblings were housed in 1 cage, with food and drinking water supplied ad libitum. Cages were enriched with aspen litter, houses, and tubes. Daily animal care was assured by professional animal care attendants.

Tamoxifen treatment

Mice at an age of 8–12 weeks were either fed tamoxifen-supplemented food or topically treated with TAM for local induction of meprin α overexpression. Food pellets supplemented with 400 mg/kg tamoxifen citrate (product identification: TD.130860) were purchased from Inotiv and fed on weekdays ad libitum. On weekends, mice were fed ad libitum with standard mouse keeping food pellets (Ssniff Spezialdiäten GmbH). For topical treatment, (Z)-4-hydroxy tamoxifen (product identification: H7904; Merck) was solved in DMSO at a concentration of 5 mg/ml. In preparation, 24 hours before the topical treatment, a 2 cm^2 area at the flank of the mice was shaved. A total volume of 50 µl TAM/cm^2 (125 µg TAM/cm^2) was directly applied to the skin of mice aged 8–12 weeks and air dried.

Skin phenotype scoring

Development of the skin phenotype in K5Mα mice was scored by the cumulative criteria listed in Table 2.

Table 2. Skin Phenotype Scoring Criteria

Criteria	Cumulative Scoring points
Reddened ears	1
Scabby ears	1
Stiff ears	1
Scabby muzzle	1
Scabby swollen muzzle with hair-loss	3
Scaly neck	1
Stiff and scabby neck with hair-loss	3
Reddened/scabby extremities (legs and tail)	1
Severe itching	5
Open wounds	3
Maximum score	20

Skin lysate preparation

Skin areas were shaved, excised, minced, snap frozen in liquid nitrogen, and 100–150 mg pulverized in a liquid nitrogen–cooled mortar. Pulverized skin samples were resuspended in lysis buffer, treated with an ultrasonic homogenizer and a Precellys 24 tissue homogenizer equipped with Cryolys adapter (Bertin Technologies). Detailed information can be found in the Supplementary Data.

Transient transfection

Plasmids used for transient transfection are listed in Table 3. Detailed information about the transfection procedure can be found in the Supplementary Data.

Cell lysis

Cells were lysed in lysis buffer and treated with an ultrasonic homogenizer (Micro Ultrasonic Cell Disruptor KT 50 with CV18 Converter and 1/8″ probe, Kontes). Detailed information can be found in the Supplementary Data.

(Co)immunoprecipitation

(Co)immunoprecipitation was performed with the Dynabeads Protein G Immunoprecipitation Kit (Invitrogen, Thermo Fisher Scientific) according to the manufacturer's instructions.

SDS-PAGE

SDS-PAGE was performed with the MINI-Protean Tetra Cell system from Bio-Rad Laboratories. Detailed information can be found in the Supplementary Data.

Western blotting

Western blotting was performed with the Criterion tank blotting system from Bio-Rad Laboratories. Detailed information can be found in the Supplementary Data.

the IP antibody (*). **(f, g)** Dermokine peptides detected by MS after IP of dermokine from lysates of HEK293T cells transfected only with a plasmid encoding C-terminally Myc-FLAG-tagged *Dmkn* compared with cells cotransfected with **(f)** *Mep1a* WT or **(g)** *Mep1a* E155A. Thresholds (—) for 0.5- and 2.0-fold changes in effect size and a $P = .05$ (2-tailed unpaired *t*-test) are shown. Peptides higher abundant (≥1.5-fold) in immunoprecipitates from cells coexpressing *Mep1a WT* and *Dmkn* than in cells only expressing *Dmkn* are marked as black dots. Putative dermokine peptide derived by meprin α cleavage (red dot). Other dermokine-derived peptides (gray dots) (n = 3 vs 3). **(h)** Meprin α (red) and dermokine (green) in skin sections from control (n = 3 per day) and K5Mα (n = 3 per day) mice. **(i)** Mean fluorescence intensity in the epidermis derived from dermokine detection shown in **h**. In skin sections from K5Mα mice, dermokine signal was exclusively quantified in meprin α–positive epidermal areas. Data are presented as mean + SEM. Statistical significance (*$P < .05$) was tested by 2-tailed unpaired *t*-test (day 1: n = 12 vs 11, $P = .0030$; day 2: n = 13 vs 5; $P = .0015$; day 3: n = 13 vs 14, $P < .0001$). **(j)** Colocalization indices in normal (black dots) and hyperplastic (red dots) epidermal regions of interest in sections from K5Mα mice correlated with the MFI for meprin α in respective regions of interest. Colocalization analysis was performed with the ImageJ plugin Colocalization Colormap on the basis of the Jaskolski's algorithm (Jaskolski et al, 2005). Nonlinear regression based on an exponential growth equation (dashed line); respective 95% confidence bands of the best-fit line (dotted line) and spearman correlation results are displayed. HEK293T, human embryonic kidney 293T; IP, immunoprecipitation; LC-MS/MS, liquid chromatography-tandem mass spectrometry; MFI, mean fluorescence intensity; RM, repeated measures; TAILS, terminal amine isotopic labeling of substrates; WT, wild-type.

Table 3. Plasmids

Vector	Transgen/Tag (species)	Transcript ID (ORF 5′−3′)	Sequence Variant
pCMV6	*Mep1a* (*Mus musculus*)	ENSMUST00000117137.8 (A95-A2338)	Wild type
pCMV6	*Mep1a* E155A (*Mus musculus*)	ENSMUST00000117137.8 (A95-A2338)	A558C
pCMV6	*Dmkn*/Myc-DDK [C-term] (*Mus musculus*)	ENSMUST00000085691.11 (A162-G1685)	Wild type
pcDNA3.1	*DMKN*/FLAG [C-term] (*Homo sapiens*)	ENST00000339686.8 (A175-G1602)	Wild type
pcDNA4/TO	*MEP1A*/Strep [N-term] /FLAG [C-term]	ENST00000230588.9 (A11-G2248)	Wild type

Abbreviations: ID, identification; ORF, open reading frame.

RNA isolation

RNA was isolated from skin samples with the RNeasy Fibrous Tissue Mini Kit (Qiagen) according to the manufacturer's instructions. RNA concentration was measured with a NanoDrop ND-1000 spectrophotometer.

Reverse transcription

Reverse transcription was performed with the RevertAid First Strand cDNA Synthesis Kit (Thermo Fisher Scientific) according to the manufacturer's instructions.

Real-time PCR

Real-time PCR analyses were carried out with a qTower^3 384G Real-time Thermocycler (Analytik Jena). PCR reactions were set up with Luna Universal qPCR Master Mix (New England Biolabs) according to the manufacturer's instructions. Melting curve analysis was run by increasing the temperature from 60 °C to 95 °C in increments of 0.5 °C. Data analysis was performed with qPCRsoft384 software, version 1.2 (Analytik Jena). Relative mRNA levels were calculated by $2^{-\Delta\Delta Ct}$-method with *Gapdh* mRNA levels as reference.

Tissue stainings

Detailed information about paraffin embedding as well as the H&E and immunofluorescence staining procedures/evaluations can be found in the Supplementary Data.

Antibodies and primer

Details about antibodies (Supplementary Table S1) and (Supplementary Table S2) primers can be found in the Supplementary Data.

Fluorogenic peptide−based activity assay

Meprin α activity in skin lysates and culture supernatants was measured by in vitro cleavage of a fluorogenic quenched peptide substrate (mca-HVANDPIW-K-ε-dnp; Genosphere Biotechnologies). Detailed information can be found in the Supplementary Data.

Proteomics

Mass spectrometry analyses were performed for characterization of alterations in the skin proteome, detection of proteolytically generated neo-N-termini, and identification of the dermokine cleavage site targeted by meprin α. Detailed information about the sample processing, data acquisition, and analyses can be found in the Supplementary Data.

Bead-based cytokine and chemokine multiplex

Cytokine and chemokine concentrations in skin lysates were measured with a customized LEGENDplex kit (BioLegend), according to the manufacturer's instructions. Measurement was performed with a FACS Symphony A1 flow cytometer (Becton Dickinson). Data analysis was conducted with the cloud-based LEGENDplex Data Analysis Software Suite. Cytokine and chemokine levels quantified in skin lysates were normalized to the respective protein concentrations of the lysates determined by BCA assay (Thermo Fisher Scientific).

Transepidermal water loss measurement

Transepidermal water loss was measured with the Multi Display Device MDD4 equipped with a Tewameter TM Nano probe (both from Courage Khazaka). Each measurement was performed in technical triplicates for at least 30 seconds each. Mean transepidermal water loss in g/h/m^2 was calculated from technical replicates for each time point for data analysis.

Transmission electron microscopy

Skin samples were dissected and immersion fixed in a mixture of 4% paraformaldehyde and 1% glutaraldehyde in 0.1 M PBS at pH 7.4 overnight. Samples were rinsed 3 times in 0.1 M sodium cacodylate buffer (pH 7.2−7.4) and osmicated using 1% osmium tetroxide in cacodylate buffer. After osmication, the tissue was dehydrated using ascending ethyl alcohol concentration steps, followed by 2 rinses in propylene oxide. Infiltration of the embedding medium was performed by immersing the pieces in a 1:1 mixture of propylene oxide and Epon and, finally, in neat Epon and hardened at 60 °C. Vertical semithin sections (0.5 µm) from the skin were prepared for light microscopy, mounted on glass slides, and stained for 1 minute with 1% toluidine blue. Consecutive ultrathin sections (60 nm) were examined in a EM902 (Zeiss). Pictures were taken with a MegaViewIII digital camera (A. Tröndle, Moorenweis, Germany).

AlphaFold 3 modeling

The structure of protein complexes was predicted using AlphaFold 3 (Abramson et al, 2024) through the official AlphaFold 3 server (https://alphafoldserver.com/about). The option "Seed" was set to auto, and the amino acid sequences used for modeling of meprin α and dermokine can be found in the Supplementary Table S4. AlphaFold 3 Model visualization and analysis were performed with PyMOL (Schrödinger).

Statistics

Statistical analyses were performed using GraphPad Prism, version 10.4.1 (GraphPad Software). Datasets were tested for Gaussian distribution and equal variance by Shapiro−Wilk and Equal Variance tests, respectively. For comparison of 2 groups comprising parametrically distributed data, 2-tailed unpaired *t*-test was conducted. In case Shapiro−Wilk test was passed but datasets failed Equal Variance test, Welch's correction was performed. Datasets that failed normality test were analyzed by 2-tailed unpaired Mann−Whitney rank sum test. In all cases, confidences level was set to 95% assuming statistically significant differences for $P < .05$. Parametric datasets comprising multiple groups were compared by 1-way ANOVA for statistical significance. Correction for multiple comparisons was conducted by Tukey's test. Nonparametric datasets comprising multiple groups were analyzed with Kruskal−Wallis

1-way ANOVA on ranks. Correction for multiple comparisons was conducted by Dunn's test. Curve fitting was performed by simple linear regression or nonlinear regression tool. Outliers were not eliminated for regression analysis, and least squares regression was chosen as fitting method. For nonlinear regression, convergence criteria were set to "medium" with automatic switch to "strict" when recommended. Maximum number of iterations was set to 1000. No weighting was performed. Regression start and end were set to "automatic," and 95% confidence bands were plotted for both linear and nonlinear regressions. For the assessment of correlations between datasets that contained 2 discontinuous dependent parametrically distributed parameters, Pearson correlation was computed. For the assessment of correlations between datasets that contained 2 discontinuous dependent nonparametrically distributed parameters, Spearman correlation was computed. Two-tailed *P*-values were calculated for a confidence level of 95%, and statistically significant differences between groups were assumed for $P < 0.05$ indicated by an asterisk (*). Differences between groups that did not reach significance level were not annotated.

ETHICAL STATEMENT AND STUDY APPROVAL

All animal experiments were carried out in accordance with the European guidelines for care and use of laboratory animals and approved by the Ministry for Agriculture, Rural Areas, Europe and Consumer Protection of the state Schleswig-Holstein (Germany) (reference V242 - 12659/2018 [30-4/18]).

DATA AVAILABILITY STATEMENT

All data needed to evaluate the conclusions of the study are present in the manuscript and/or the Supplementary Materials. The mass spectrometry proteomics data have been deposited to the ProteomeXchange Consortium through the PRIDE (Perez-Riverol et al, 2025) partner repository (https://www.ebi.ac.uk/pride/) with the dataset identifier PXD063928. Supplementary data available through the journals' website also include the following: Supplementary data (proteins significantly higher abundant in the skin of K5Mα mice on day 3 after topical tamoxifen treatment), Supplementary Materials and Methods (detailed description of all methods). For any further questions regarding protocols and materials, please contact SR (srueffer@biochem.uni-kiel.de).

ORCIDs

Sascha Rüffer: http://orcid.org/0009-0000-0181-0388
Christoph Becker-Pauly: http://orcid.org/0000-0002-5100-9916
Vasco Köhling: http://orcid.org/0009-0002-4934-0439
Florian Peters: http://orcid.org/0000-0002-8529-2326
Fred Armbrust: http://orcid.org/0000-0002-3331-5522
Silje Beckinger: http://orcid.org/0009-0009-3263-1812
Cynthia Bülck: http://orcid.org/0000-0002-8354-6177
Vahap Canbay: http://orcid.org/0000-0002-5218-2315
Inken Harder: http://orcid.org/0000-0002-3079-0440
Marion Mengel: http://orcid.org/0000-0002-4876-008X
Malina Rüffer: http://orcid.org/0009-0003-8443-223X
Kira Bickenbach: http://orcid.org/0000-0001-5079-0512
Konstantinos Kalogeropoulos: http://orcid.org/0000-0003-3907-9281
Michaela Schweizer: http://orcid.org/0000-0001-5062-328X
Neele Schumacher: http://orcid.org/0000-0002-8389-0365
Nathalie Jonca: http://orcid.org/0000-0003-3602-0102
Michael Haase: http://orcid.org/0000-0002-5897-0320
Ulrich auf dem Keller: http://orcid.org/0000-0002-3431-7415

CONFLICT OF INTEREST

The authors state no conflict of interest.

ACKNOWLEDGMENTS

The mouse line C57BL/6J-KRT5$^{tm1.1\text{-}CreERT2}$;ROSA26$^{Stop\text{-}mMep1a}$ is covered by a patent held by CB-P and FP under the patent number EP20160475.8 (02.03.3030) W0 2021/175738 2021/36 (10.09.2021) (Animal models for hyperkeratosis and sepsis). SR is the guarantor for this study. The authors thank Lennard Arp (former technical assistant at the Biochemical Institute, Christian-Albrechts-University of Kiel) and Alexander Bitter (technical assistant at the Biochemical Institute, Christian-Albrechts-University of Kiel) for excellent technical assistance as well as Hila Emmert (former professor at the Clinic for Dermatology, Venerology and Allergology, University Medical Center Schleswig-Holstein, Kiel) for productive scientific exchange. This study was supported by the Deutsche Forschungsgemeinschaft through the Collaborative Research Centre 877 (Proteolysis as a Regulatory Event in Pathophysiology, Project A9) and Project 5098655290 (Knock-in mouse models for the characterization of meprin metalloproteases in hyperkeratosis, inflammation and systemic sclerosis) (both to CBP) as well as the Christian-Albrechts-University Kiel by intramural funding K126444 (meprin α, a novel molecular driver and potential therapeutic target in sepsis) and the Cluster of Excellence EXC 2167 (Precision Medicine in Chronic Inflammation) for the mini proposal "Characterization of a genetic mouse model for systemic inflammation: A novel tool to unravel molecular hallmarks and therapeutic targets in sepsis?" (both to SR). UadK is deceased (August 23, 2023)

AUTHOR CONTRIBUTIONS

Conceptualization: VK, FP, CB-P, SR; Data Curation: VK, FP, SR; Formal Analysis: VK, VC, KK, MS, SR, CB-P; Funding Acquisition: CB-P, SR; Investigation: VK, FP, IG, EF, NB, FA, SB, CB, VC, MM, MR, KB, KK, MS, ML, NS, SR; Methodology: MH, RN, FP, VK, IG, NJ, IH, ML, SB, SR, VC, KK, UadK; Project Administration: CB-P, SR; Resources: VC, IH, KK, MS, NS, NJ, MH, RN, UadK, CB-P, SR; Supervision: CB-P, SR; Writing − Original Draft Preparation: SR; Writing − Review and Editing: VK, FP, IG, EF, NB, FA, SB, CB, VC, IH, MM, MR, KB, KK, MS, ML, NS, NJ, MH, RN, UadK, CB-P, SR

DECLARATION OF GENERATIVE ARTIFICIAL INTELLIGENCE (AI) OR LARGE LANGUAGE MODELS (LLMs)

The author(s) did not use AI/LLM in any part of the research process and/or manuscript preparation.

SUPPLEMENTARY MATERIAL

Supplementary material is linked to the online version of the paper at www.jidonline.org, and at 10.1016/j.jid.2026.01.034.

REFERENCES

Abramson J, Adler J, Dunger J, Evans R, Green T, Pritzel A, et al. Accurate structure prediction of biomolecular interactions with AlphaFold 3. Nature 2024;630:493−500.

Becker C, Kruse MN, Slotty KA, Köhler D, Harris JR, Rösmann S, et al. Differences in the activation mechanism between the alpha and beta subunits of human meprin. Biol Chem 2003;384:825−31.

Becker-Pauly C, Barré O, Schilling O, Auf Dem Keller U, Ohler A, Broder C, et al. Proteomic analyses reveal an acidic prime side specificity for the astacin metalloprotease family reflected by physiological substrates. Mol Cell Proteomics 2011;10:M111.009233.

Becker-Pauly C, Höwel M, Walker T, Vlad A, Aufenvenne K, Oji V, et al. The alpha and beta subunits of the metalloprotease meprin are expressed in separate layers of human epidermis, revealing different functions in keratinocyte proliferation and differentiation. J Invest Dermatol 2007;127:1115−25.

Bülck C, Nyström EEL, Koudelka T, Mannbar-Frahm M, Andresen G, Radhouani M, et al. Proteolytic processing of galectin-3 by meprin metalloproteases is crucial for host-microbiome homeostasis. Sci Adv 2023;9:eadf4055.

Candi E, Oddi S, Paradisi A, Terrinoni A, Ranalli M, Teofoli P, et al. Expression of transglutaminase 5 in normal and pathologic human epidermis. J Invest Dermatol 2002;119:670−7.

Chavanas S, Bodemer C, Rochat A, Hamel-Teillac D, Ali M, Irvine AD, et al. Mutations in SPINK5, encoding a serine protease inhibitor, cause netherton syndrome. Nat Genet 2000;25:141−2.

De Koning HD, Van Den Bogaard EH, Bergboer JG, Kamsteeg M, Van Vlijmen-Willems IM, Hitomi K, et al. Expression profile of cornified envelope structural proteins and keratinocyte differentiation-regulating proteins during skin barrier repair. Br J Dermatol 2012;166:1245−54.

de Veer SJ, Furio L, Harris JM, Hovnanian A. Proteases: common culprits in human skin disorders. Trends Mol Med 2014;20:166−78.

Hahn D, Pischitzis A, Roesmann S, Hansen MK, Leuenberger B, Luginbuehl U, et al. Phorbol 12-myristate 13-acetate-induced ectodomain shedding and phosphorylation of the human Meprinbeta metalloprotease. J Biol Chem 2003;278:42829−39.

Hasegawa M, Higashi K, Matsushita T, Hamaguchi Y, Saito K, Fujimoto M, et al. Dermokine inhibits ELR(+)CXC chemokine expression and delays early skin wound healing. J Dermatol Sci 2013a;70:34–41.

Hasegawa M, Higashi K, Yokoyamea C, Yamamoto F, Tachibana T, Matsushita T, et al. Altered expression of dermokine in skin disorders. J Eur Acad Dermatol Venereol 2013b;27:867–75.

Herzog C, Haun RS, Ludwig A, Shah SV, Kaushal GP. ADAM10 is the major sheddase responsible for the release of membrane-associated meprin A. J Biol Chem 2014;289:13308–22.

Higashi K, Hasegawa M, Yokoyama C, Tachibana T, Mitsui S, Saito K. Dermokine-β impairs ERK signaling through direct binding to GRP78. FEBS Lett 2012;586:2300–5.

Jäckle F, Schmidt F, Wichert R, Arnold P, Prox J, Mangold M, et al. Metalloprotease meprin β is activated by transmembrane serine protease matriptase-2 at the cell surface thereby enhancing APP shedding. Biochem J 2015;470:91–103.

Jaskolski F, Mulle C, Manzoni OJ. An automated method to quantify and visualize colocalized fluorescent signals. J Neurosci Methods 2005;146:42–9.

Kawahira K. Immunohistochemical staining of proliferating cell nuclear antigen (PCNA) in malignant and nonmalignant skin diseases. Arch Dermatol Res 1999;291:413–8.

Kim SA, Ryu YW, Kwon JI, Choe MS, Jung JW, Cho JW. Differential expression of cyclin D1, Ki-67, pRb, and p53 in psoriatic skin lesions and normal skin. Mol Med Rep 2018;17:735–42.

Kishibe M. Physiological and pathological roles of kallikrein-related peptidases in the epidermis. J Dermatol Sci 2019;95:50–5.

Komatsu N, Saijoh K, Kuk C, Shirasaki F, Takehara K, Diamandis EP. Aberrant human tissue kallikrein levels in the stratum corneum and serum of patients with psoriasis: dependence on phenotype, severity and therapy. Br J Dermatol 2007;156:875–83.

Kruppa D, Peters F, Bornert O, Maler MD, Martin SF, Becker-Pauly C, et al. Distinct contributions of meprins to skin regeneration after injury - Meprin α a physiological processer of pro-collagen VII. Matrix Biol Plus 2021;11:100065.

Leclerc EA, Huchenq A, Kezic S, Serre G, Jonca N. Mice deficient for the epidermal dermokine β and γ isoforms display transient cornification defects. J Cell Sci 2014;127:2862–72.

Marchand P, Tang J, Johnson GD, Bond JS. COOH-terminal proteolytic processing of secreted and membrane forms of the alpha subunit of the metalloprotease meprin A. Requirement of the I domain for processing in the endoplasmic reticulum. J Biol Chem 1995;270:5449–56.

Matsui T, Hayashi-Kisumi F, Kinoshita Y, Katahira S, Morita K, Miyachi Y, et al. Identification of novel keratinocyte-secreted peptides dermokine-alpha/- beta and a new stratified epithelium-secreted protein gene complex on human chromosome 19q13.1. Genomics 2004;84:384–97.

McGowan K, Coulombe PA. The wound repair-associated keratins 6, 16, and 17. Insights into the role of intermediate filaments in specifying keratinocyte cytoarchitecture. Subcell Biochem 1998;31:173–204.

Morizane S, Sunagawa K, Nomura H, Ouchida M. Aberrant serine protease activities in atopic dermatitis. J Dermatol Sci 2022;107:2–7.

Ohler A, Debela M, Wagner S, Magdolen V, Becker-Pauly C. Analyzing the protease web in skin: meprin metalloproteases are activated specifically by KLK4, 5 and 8 vice versa leading to processing of proKLK7 thereby triggering its activation. Biol Chem 2010;391:455–60.

Ovaere P, Lippens S, Vandenabeele P, Declercq W. The emerging roles of serine protease cascades in the epidermis. Trends Biochem Sci 2009;34:453–63.

Perez-Riverol Y, Bandla C, Kundu DJ, Kamatchinathan S, Bai J, Hewapathirana S, et al. The PRIDE database at 20 years: 2025 update. Nucleic Acids Res 2025;53:D543–53. https://pubmed.ncbi.nlm.nih.gov/39494541/.

Peters F, Rahn S, Mengel M, Scharfenberg F, Otte A, Koudelka T, et al. Syndecan-1 shedding by meprin β impairs keratinocyte adhesion and differentiation in hyperkeratosis. Matrix Biol 2021;102:37–69.

Peters F, Scharfenberg F, Colmorgen C, Armbrust F, Wichert R, Arnold P, et al. Tethering soluble meprin α in an enzyme complex to the cell surface affects IBD-associated genes. FASEB J 2019;33:7490–504.

Rösmann S, Hahn D, Lottaz D, Kruse MN, Stöcker W, Sterchi EE. Activation of human meprin-alpha in a cell culture model of colorectal cancer is triggered by the plasminogen-activating system. J Biol Chem 2002;277:40650–8.

Sotiropoulou G, Zingkou E, Pampalakis G. Reconstructing the epidermal proteolytic cascades in health and disease. J Pathol 2022;257:545–60.

Usui ML, Underwood RA, Mansbridge JN, Muffley LA, Carter WG, Olerud JE. Morphological evidence for the role of suprabasal keratinocytes in wound reepithelialization. Wound Repair Regen 2005;13:468–79.

Utsunomiya A, Chino T, Utsunomiya N, Luong VH, Tokuriki A, Naganuma T, et al. Homeostatic function of dermokine in the skin barrier and inflammation. J Invest Dermatol 2020;140:838–49.e9.

Werny L, Grogro A, Bickenbach K, Bülck C, Armbrust F, Koudelka T, et al. MT1-MMP and ADAM10/17 exhibit a remarkable overlap of shedding properties. FEBS J 2023;290:93–111.

Wichert R, Ermund A, Schmidt S, Schweinlin M, Ksiazek M, Arnold P, et al. Mucus detachment by host metalloprotease meprin β requires shedding of its inactive pro-form, which is abrogated by the pathogenic protease RgpB. Cell Rep 2017;21:2090–103.

Zhang X, Yin M, Zhang LJ. Keratin 6, 16 and 17-critical barrier alarmin molecules in skin wounds and psoriasis. Cells 2019;8:807.

SUPPLEMENTARY MATERIALS AND METHODS

Generation of C57BL/6J-KRT5$^{tm1.1\text{-}CreERT2}$;ROSA26$^{Stop\text{-}mMep1a}$ mice

Meprin α knock-in mice (C57BL/6J-ROSA26$^{Stop\text{-}mMep1a}$) were generated at the Transgenic Core Facility of the Max Planck Institute for Molecular Cell Biology and Genetics (Dresden, Germany). In advance, murine meprin α cDNA (transcript identification: ENSMUST00000117137.8; A95-G2335) was cloned into pCAG-ROSA-IRES-EGFP–targeting vector. Murine JM8A1.N3 embryonic stem cells (Pettitt et al, 2009) were transfected by electroporation and clones selected that incorporated the transgenic construct (CAG-loxP-Neo^{R}-STOP-loxP-mMep1a-HA-IRES-GFP) by homologous recombination into the Rosa26 locus of their genome. Suitable embryonic stem cell clones were transplanted by laser-assisted microinjection into C57BL6/NCrl morula stages 2.5 days after coitum (Poueymirou et al, 2007) for fertilization of recipient female mice. Sperms of chimeric male offspring were screened by short tandem repeat analysis for transgenic proportion, and suitable samples were selected for in vitro fertilization. Heterozygous offspring was crossed with B6N.129S6(Cg)-Krt5$^{tm1.1(cre/ERT2)Blh}$/J mice (Van Keymeulen et al, 2011) (Jackson Laboratory, stock number 029155) to generate C57BL/6J-KRT5$^{tm1.1\text{-}CreERT2}$;ROSA26$^{Stop\text{-}mMep1a}$ mice (patent application EP20160475.8/W0 2021/175738 A1). Mice that carried homozygous mMep1a construct within the Rosa26 locus and were either heterozygous with the information for the Cre recombinase/modified estrogen receptor fusion protein (CreER^{T2}+/−; K5Mα) or not (CreER^{T2}−/−; control) were used for subsequent experiments. To breed only mice with a heterozygous and not homozygous CreER^{T2} status, CreER^{T2}-positive mice were only crossed with CreER^{T2}-negative mice.

Genotyping

For genotyping of C57BL/6J-KRT5$^{tm1.1\text{-}CreERT2}$;ROSA26$^{Stop\text{-}mMep1a}$ mice, genomic DNA was extracted from ear punches using the DirectPCR Lysis Reagent Tail (Peqlab Biotechnologies) according to the manufacturer's instructions. For subsequent PCR reaction, 2 μl lysate was added to a total reaction volume of 30 μl containing DreamTaq DNA polymerase (80 IU/ml), 3 μl DreamTaq Green Buffer (10×), 2 mM deoxynucleoside triphosphates, and respective primers at a concentration of 0.4 μM. Analysis of the Rosa26 locus zygosity for wild-type sequence and transgenic sequence was performed using the following primer set: forward (wild-type/transgenic) 5′-aaagtcgctctgagttgttatc-3′, reverse (wild-type) 5′- gatatgaagtactgggctctt-3′, and reverse (transgenic) 5′-tgtcgcaaattaactgtgaatc-3′. PCR products at a size of 570 bp and 380 bp indicated wild-type and transgenic Rosa26 locus, respectively. Analysis of the CreER^{T2} status was performed using the following primer set: forward 5′- ggttcgcaagaacctgatggacat-3′ and reverse 5′- gctagagcctgttttgcacgttca-3′. A PCR product at a size of 342 bp indicated insertion of the CreER^{T2} construct downstream of the keratin 5 promotor. The following PCR programs were run for genotyping of Rosa26 and CreER^{T2} status: (i) Rosa26: 95 °C for 3 minutes, 35 cycles (95 °C for 30 seconds, 56 °C for 30 seconds, 72 °C for 50 seconds), 72 °C for 10 minutes and (ii) CreER^{T2}: 95 °C for 5 minutes, 30 cycles (95 °C for 30 seconds, 56 °C for 30 seconds, 72 °C for 15 seconds), 72 °C for 10 minutes.

Skin lysate preparation

After mice were killed, respective skin areas were shaved, excised, minced, snap frozen in liquid nitrogen, and 100–150 mg pulverized in a liquid nitrogen–cooled mortar. Pulverized skin samples were transferred to a 1.5 ml tube with a screw cap. Next, 400 μl lysis buffer (50 mM Tris-hydrogen chloride, 150 mM sodium chloride, 1% [v/v] Triton X-100, 1% [w/v] SDS, 2 mM EDTA, cOmplete Protease Inhibitor Cocktail EDTA-free, PhosSTOP Phosphatase Inhibitor Cocktail, pH 6.8) were added to the pulverized skin. Skin lysates intended for meprin α activity measurements were generated in lysis buffer without EDTA and SDS. Afterward, lysates were treated in 3 cycles with an ultrasonic homogenizer (Micro Ultrasonic Cell Disruptor KT 50 with CV18 Converter and 1/8″ probe, Kontes) at 20% power 5 × 2 seconds per cycle with a cooling phase of 5 minutes between each cycle. Then, ceramic beads were added, and lysates were subjected to a Precellys 24 tissue homogenizer equipped with Cryolys adapter (Bertin Technologies). Liquid nitrogen–cooled lysis was performed in 3 cycles each at 6500 r.p.m. for 30 seconds with a break of 30 seconds between cycles. Finally, lysates were incubated for 1 hour on ice and centrifuged at 20,000*g* and 4 °C for 30 minutes, and supernatants were transferred to fresh tubes. Protein concentrations were determined by BCA assay according to the manufacturer's instructions (Pierce BCA Assay Kit, Thermo Fisher Scientific), and lysates were stored at −20 °C until subsequent analysis.

Transient transfection

In preparation, 3 × 10^6 human embryonic kidney 293T (HEK293T) cells were seeded in 10 ml DMEM + GlutaMAX (Gibco, Thermo Fisher Scientific) supplemented with 10% (v/v) heat-inactivated fetal calf serum (Thermo Fisher Scientific), 100 U/ml penicillin, and 100 μg/ml streptomycin (Gibco, Thermo Fisher Scientific) into a 10-cm (58 cm^2) culture dish. HEK293T cells were cultured for 24 hours at 37 °C, 5% carbon dioxide, and 85% relative humidity. For transient transfection, 3 μl polyethylenimine (Merck) per microgram DNA were mixed in DMEM with respective plasmids. After incubation for 20 minutes at room temperature, transfection mix was added dropwise to the culture supernatant under constant agitation of the culture dish. Twenty-four hours after transfection, culture medium was removed, cells were washed with PBS, and 5 ml DMEM + GlutaMAX supplemented with 100 U/ml penicillin and 100 μg/ml streptomycin were added to the cells. Additional 24 hours later, supernatants were collected, and cells were subjected to lysis.

Cell lysis

Culture medium of HEK293T cells was removed, and cells were washed twice with PBS. Cells were taken up in lysis buffer (50 mM Tris-hydrogen chloride, 150 mM sodium chloride, 1% [v/v] Triton X-100, 1% [w/v] SDS, 2 mM EDTA, cOmplete Protease Inhibitor Cocktail EDTA-free, PhosSTOP Phosphatase Inhibitor Cocktail, pH 6.8) and treated in 3 cycles with an ultrasonic homogenizer (Micro Ultrasonic Cell Disruptor KT 50 with CV18 Converter and 1/8″ probe, Kontes) at 20% power 3 × 2 seconds per cycle with a cooling phase of 5 minutes between each cycle. Cell lysates intended

for activity measurements were generated in lysis buffer without EDTA and SDS. Finally, lysates were incubated for 1 hour on ice and centrifuged at 20,000*g* and 4°C for 30 minutes, and supernatants were transferred to fresh tubes. Protein concentrations were determined by BCA assay according to the manufacturer's instructions (Pierce BCA Assay Kit, Thermo Fisher Scientific), and lysates were stored at −20 °C until subsequent analysis.

SDS-PAGE

In preparation, lysates were adjusted to an equal protein concentration with respective lysis buffer and diluted 5:1 with 5X SDS-PAGE sample buffer (250 mM Tris-hydrogen chloride, 350 mM SDS, 7.5 mM bromophenol blue, 50% [v/v] glycerol, 100 mM dithiothreitol in double-distilled water, pH 6.8). Samples were denatured by incubation for 10 minutes at 95 °C. Discontinuous SDS-PAGE was carried out with a polyacrylamide content of 7.5, 10, 12, 14, or 18% in the separating gel dependent on the desired resolution. Electrophoresis was run at constant voltage of 90 V in the collecting gel and 120 V in the separating gel. PageRuler Prestained Protein Ladder (Thermo Fisher Scientific) was used as a molecular weight marker.

Western blotting

For the transfer onto a polyvinylidene fluoride membrane in tank blot buffer (25 mM Tris-hydrogen chloride, 200 mM glycine, 20% [v/v] methanol in double-distilled water, pH 8.3), a constant current of 2.5 mA/cm^2 was applied for 2 hours at 4 °C. Afterward, membranes were washed for 5 minutes in Tris buffered saline with Tween 20 (TBS-T) (25 mM Tris-hydrogen chloride, 150 mM sodium chloride, 0.05% [v/v] Tween-20 in double-distilled water, pH 7.5) and blocked by incubation in 5% (w/v) skim milk powder in TBS-T for 1 hour at room temperature. Then, membranes were incubated overnight on a roller mixer at 4 °C with respective primary antibodies diluted in either 5% (w/v) skim milk powder/TBS-T or 5% (w/v) BSA/TBS-T. The following day, membranes were washed twice in TBS-T, once in Tris buffered saline, and incubated for 1 hour on a roller mixer at room temperature with horse radish peroxidase—conjugated secondary antibodies in 5% (w/v) skim milk powder/TBS-T. After further washing steps, membranes were incubated for 2 minutes in WesternBright ECL HRP substrate (Advansta), and chemiluminescence was detected with the Amersham ImageQuant 800 biomolecular imager (Cytiva). Image analysis was performed with the ImageQuant TL software version 8.2 (GE Healthcare).

Paraffin embedding and tissue sectioning

Excised skin samples were fixed by incubation in 4% (w/v) paraformaldehyde/PBS for 48 hours at room temperature. Afterward, skin samples were watered in tap water for 5 hours. Tissue dehydration by ascending alcohol series started with 50% ethanol overnight and proceeded with 70% ethanol for 1 hours, 95% ethanol for 30 minutes, 95% ethanol for 1 hour, 100% ethanol for 1.5 hours, 100% ethanol for 2 hours, and xylene for 1.5 hours and ended by incubation in xylene for 1.5 hours. Dehydrated skin samples were soaked with paraffin at 60 °C overnight. Embedded skin samples were cut with a rotary microtome HistoCore BIOCUT (Leica Biosystems) into 5-µm sections and fixed on slides for subsequent staining.

H&E staining

Skin sections were stained with Mayer's hemalum (Merck) and 1% aqueous Eosin-G (Roth). Therefore, skin sections were deparaffinized in xylene and rehydrated by a descending alcohol series (2× 100%, 95%, 70%, 50% ethanol). Then, skin sections were rinsed in distilled water and incubated for 10 minutes in filtered Mayer's hemalum solution. Afterward, skin sections were rinsed twice with distilled water, rinsed once with distilled water acidified with hydrogen chloride, rinsed twice with distilled water, and incubated for 5 minutes in lukewarm tap water for hemalum development. Then, skin sections were rinsed twice with distilled water and incubated for 5 minutes in filtered aqueous Eosin-G solution acidified with acetic acid. After skin sections were rinsed once with distilled water, sections were dehydrated by an ascending alcohol series (70%, 90%, 96%, 2× 100% ethanol, 2× xylene), embedded in Entellan mounting medium (Merck), and sealed with a coverslip. Imaging was performed with the Aperio CS2 brightfield scanner (Leica Biosystems) at ×40 magnification. Aperio ImageScope software, version 12.4.6.5003 (Leica Biosystems), was used for visualization and image analyses.

Immunofluorescence staining

Skin sections were deparaffinized in xylene, rehydrated by a descending alcohol series (2× 100%, 95%, 70%, 50% ethanol) rinsed with distilled water, and incubated for 10 minutes in PBS. Heat-induced antigen retrieval was conducted in preheated citric acid buffer (2 mM citric acid, 8 mM trisodium citrate trihydrate, 0.05% Tween-20, pH 6.0) for 20 minutes in a steamer. Afterward, tissue sections were cooled to room temperature, washed 3 times in PBS for 5 minutes each, and blocked by incubation in 5% (w/v) IgG-free BSA/PBS for 1 hour at room temperature in a wet chamber. Then, skin sections were incubated overnight at 4 °C with respective primary antibodies diluted in 1% (w/v) IgG-free BSA/PBS in a wet chamber. Afterward, skin sections were washed thrice and incubated in for 1 hour at room temperature in a wet chamber with fluorochrome-conjugated secondary antibodies in 1% (w/v) IgG-free BSA/PBS supplemented with 1.5 µg/ml DAPI. Finally, skin sections were washed 3 times, rinsed with distilled water, embedded in Fluorescence Mounting Medium (Dako), and sealed with a cover slip. Image acquisition was performed with the MICA microhub fluorescence microscope (Leica Biosystems). Noise reduction was conducted by instant computational clearing in THUNDER mode (Walter and Ziesche, 2019). For visualization and image analysis, Leica Application Suite X software (Leica Biosystems) and ImageJ (National Institutes of Health) were used.

Colocalization analysis

Colocalization analyses of meprin α and dermokine in immunofluorescence images were performed with the ImageJ plugin "Colocalization Colormap" (https://sites.google.com/site/colocalizationcolormap/home). The plugin was programmed by Adam Gorlewicz (Nencki Institute of Experimental Biology, Warsaw, Poland) and is available as freeware through the GitHub repository (https://github.com/AdamGorlewicz/Colocalization-colormap/tree/master). The plugin utilizes an algorithm reported by Jaskolski et al (2005)

(for visualization and quantification of colocalized signals in fluorescence microscopy images). In brief, regions of interest within the epidermis were marked with the Freehand Selection tool provided by ImageJ in 8-bit gray scale images of channels for detection of meprin α and dermokine. Colocalization Colormap plugin was run with "Autothreshold" option selected. Colocalization indices were computed by the plugin and output as the Index of Correlation (Icorr) with values ranging from 0 (no overlap) to 1 (100% overlap).

Fluorogenic peptide–based activity assay

Meprin α activity in skin lysates and culture supernatants was measured by in vitro cleavage of a fluorogenic quenched peptide substrate (mca-HVANDPIW-K-ε-dnp; Genosphere Biotechnologies). The peptide is specifically cleaved by meprin α (Peters et al, 2019), N-terminal conjugated with a fluorophore (7-methyloxycoumarin-4-yl), and C-terminal conjugated with a quencher (K-ε-2,4-dinitrophenyl). Briefly, 100 μg skin lysate or 100 μl ultracentrifuged (2 hours; 20,818g; 4 °C) culture supernatant was mixed with 5 μM peptide substrate in a white 96-well flat bottom plate to reaction volume of 100 μl with PBS. For activation of meprin α in culture supernatants, 50 μg/ml bovine trypsin were added to the reaction volume. For inhibition of meprin α in culture supernatants, 10 μM actinonin was added to the reaction volume. Fluorescence intensity was measured for 2 hours every 30 seconds at 37 °C with a Tecan Spark spectrofluorophotometer (Tecan) with an excitation wavelength of 320 nm at an emission wavelength of 405 nm. All samples were measured in technical duplicates. Mean temporal changes in relative fluorescence intensities were calculated by linear regression in equal timeframes. Relative fluorescence intensity change per minute was defined as meprin α activity.

Terminal amine isotopic labeling of substrates

In preparation for mass spectrometry analyses, proteins in skin lysates were precipitated by methanol and chloroform. In brief, methanol was added to skin lysates in a ratio of 4:1 and thoroughly mixed. Then, chloroform was added in a ratio of 1:5 and thoroughly mixed. Afterward, distilled water was added in a ratio of 1:2, and lysates were mixed and centrifuged for 2 minutes at 14,000*g*. Top layer was removed, and interface layer was separated and mixed with methanol at a ratio of 1:4. Finally, samples were centrifuged for 3 minutes at 14,000*g*, and methanol was discarded. Remaining sediment was dried and stored at −80 °C until further processing.

Sample processing and N-terminal enrichment were performed according to the N-terminomics HUNTER protocol (Weng et al, 2019), modified for Tandem Mass Tag multiplexing (Meyer et al, 2021) with minor adaptations. Briefly, 50 μg protein per sample was resuspended in 100 μl TAILS buffer (250 mM 4-[2-hydroxyethyl]-1-piperazineethanesulfonic acid [HEPES], pH 7.8, 2.5 M guanidine hydrochloride) in protein low-bind tubes. Reduction and alkylation were performed by adding Tris-(2-carboxyethyl)-phosphine and freshly prepared chloroacetamide to final concentrations of 10 and 40 mM, respectively, followed by incubation at 95 °C for 10 minutes at 600 r.p.m. Each vial of 16-plex TMTpro (Thermo Fisher Scientific) label (200 μg) was dissolved in 55 μl anhydrous DMSO, mixed with an equal volume of sample, and incubated at room temperature for approximately 1 hour. The labeling reaction was quenched by adding 1 M ammonium bicarbonate (final concentration 100 mM) and incubating for 30 minutes at room temperature. Labeled samples were combined and aliquoted into 1.5 ml protein low-bind tubes (approximately 250 μl each), and magnetic beads (Sera-Mag hydrophilic and hydrophobic carboxylate-modified SpeedBeads, Cytiva) were added at a 1:10 (protein:beads, w/w) ratio. Samples were incubated in 80% ethanol on a shaker (800 r.p.m.) at room temperature for 15 minutes, followed by washing with 90% ethanol. Beads were then resuspended in 100 mM HEPES (pH 7.8) for final protein concentration of 1 μg/μl. Trypsin digestion (1:50 trypsin:protein, w/w) occurred overnight at 37 °C at 350 r.p.m. After digestion, samples were mixed with equal volumes of 100 mM HEPES containing 2 M guanidine hydrochloride, incubated at 85 °C for 5 minutes at 1000 r.p.m., and centrifuged briefly. The supernatant was transferred, and 10% was set aside as a nonpullout control stored at −20 °C. The remaining peptides underwent depletion of tryptic peptides by adding undecanal (50:1 undecanal:peptide, w/w) and sodium cyanoborohydride (50 mM final concentration), adjusting pH to 6–7, and incubating at 50 °C for 1.5 hours at 450 r.p.m. The reaction was acidified to pH 1.5–2.5 with Buffer H′ (40% ethanol, 5% trifluoroacetic acid [TFA]), adjusted to 600 μl with Buffer H (40% ethanol, 1% TFA), and loaded onto activated SepPak columns to isolate enriched N-terminal peptides (pullout). Both nonpullout and pullout samples were desalted using activated SepPak columns (Waters), equilibrated with Buffer A′ (3% acetonitrile, 1% TFA), washed with Buffer A (0.1% formic acid), and eluted with Buffer B (80% acetonitrile, 0.1% formic acid). The eluates were dried in a speed vacuum concentrator and resuspended in Buffer A* (2% acetonitrile, 1% TFA). Peptide concentrations were measured, and 500 ng peptides per sample were loaded onto EvoTips (EvoSep) for subsequent liquid chromatography-tandem mass spectrometry analysis.

TAILS data acquisition

Samples were measured using the EvoSep One platform (Evosep) coupled to an Orbitrap Exploris 480 mass spectrometer with a FAIMSpro interface (Thermo Fisher Scientific). Peptides were separated on an EV1106 C18 column (15 cm × 150 μm, 1.9 μm diameter, Evosep) using the Whisper100 nanoflow system with a 15 SPD (samples per day) method, comprising an 88-minute gradient. Eluting peptides were injected into the mass spectrometer through a 20-μm fused silica emitter (EV1087, Evosep) at a static voltage of 2300 V, with a carrier gas flow of 3.6 l/min and an ion transfer tube temperature of 240 °C. FAIMS was operated at 2 CVs, −50 and −70, with cycle time of 2 seconds each. MS1 scans were acquired at 120,000 resolution across a mass range of 375–1500 m/z, maximum injection time of 246 ms, normalized AGC target of 1.2e6, and RF Lens at 40%. For data-dependent scans, filters included charged ions (charge states 2–7), dynamic exclusion for 60 seconds with a ±10 ppm tolerance, minimum intensity threshold of 5e3, and precursor fit threshold of 0.7. Data-dependent MS2 scans were acquired in centroid mode at 60,000 resolution, with an isolation window of 0.7 m/z; first mass at 110 m/z; higher-energy collisional dissociation fragmentation at 34%

normalized collision energy; AGC target of 375,000; and a maximum injection time of 118 ms. Raw data were analyzed using Proteome Discoverer (version 2.4), searching against the mouse proteome database from Uniprot. Search parameters included semitryptic specificity, 2 maximum missed cleavages, dynamic modifications (methionine oxidation [+15.995], asparagine deamidation [+0.984], TMTpro labeling [+304.207], and protein N-terminal acetylation [+42.011]), and static modifications (cysteine carbamidomethylation [+57.021] and lysine TMTpro labeling). Peptide-spectrum matching utilized Sequest HT, with false discovery rate controlled by Percolator at 1% strict and 5% relaxed thresholds. Peptides and proteins were quantified using the Reporter Ion Quantifier node and normalized to the total peptide amount per channel. Exported peptide group and protein reports underwent downstream analysis with CLIPPER 2.0 (Kalogeropoulos et al, 2024).

TAILS data filtering for identification of potential meprin α substrates

For the identification of peptides potentially generated by meprin α, TAILS data were filtered according to the following scheme. First, all peptides without an N-terminal Tandem Mass Tag label and those that did not contain the canonical N-terminal methionine were filtered out. Next, peptides derived from proteins annotated as plasma membrane or extracellular localized were filtered by Gene Ontology annotations. Subsequently, peptides that were higher abundant in the skin of K5Mα than in the control mice were filtered by cutoff values. For this purpose, n-fold differences of the mean were calculated. In order not to overlook proteolytic events that might cause only minor changes in relative peptide abundance but have a relevant impact, a lower threshold on days 1 and 2 (≥1.2-fold) than on day 3 (≥1.5-fold) was defined. These peptides were filtered for the extracellular proteolytic accessibility of their N-terminus by the data deposited in the UniProt data base to ensure that these peptides could be potentially generated by meprin α. Afterward, peptides derived from proteins that are potentially localized in the epidermis were identified by literature search. Here, peptides derived from proteins that are not localized in the epidermis by high certainty, for example, muscle specific proteins, were excluded from further analyses. Next, the peptides' putative cleavage site was examined with regard to the cleavage specificity of meprin α. Therefore, peptides that contained an aspartate or glutamate residue in P1, P1′, or P2′ position or a proline residue in P2′ were filtered. Then, the amino acid sequence from P3 to P3′ position of the peptides was rated with regard to amino acids preferred by human meprin α. Here, the relative abundance of the respective amino acids annotated in the MEROPS database (https://www.ebi.ac.uk/merops/) was used. As readout, a Peptide Score was calculated, which represents the sum of the likelihood values for each amino acid in positions P3 to P3′ (Supplementary Table S3). A Peptide Score ≥300 was defined as a cutoff by calculating the median value of all analyzed peptides. In the same step, peptides that contained a highly disfavored amino acid (likelihood value <10) in positions P2 to P2′ and those that were derived by removal of a signal peptide were excluded. Finally, the raw signal intensities and changes in the signal intensities detected by TAILS were defined as selection criteria. Selection criteria included that signal intensities of candidate peptides have to increase in skin samples from K5Mα mice from day 1 to 2 or 3 and that absolute intensity value must be greater than in skin samples from control mice on day 1, 2, or 3 after TAM treatment.

Cleavage site identification

Dynabeads magnetic beads from coimmunoprecipitation were resuspended in 4 M digestion buffer (4 M guanidine hydrochloride and HEPES [pH 8.0]), and an on-bead digestion was carried out. Cysteine reduction was carried out using Tris-(2-carboxyethyl)-phosphine (5 mM final concentration) and alkylation with chloroacetamide (20 mM final concentration) both carried out at 400 r.p.m. at 65 °C for 30 minutes. After reduction and alkylation, samples were diluted 8-fold to reduce the guanidine hydrochloride concentration to 0.5 M using 100 mM HEPES (pH 8.0), and LysC (Wako) (1:100) was added for 4 hours followed by overnight digestion with sequencing-grade modified trypsin (1:50) (Sigma). The reaction was quenched using 1% TFA. The beads were centrifuged at 14,000*g* for 10 minutes, and the supernatant was transferred to a fresh tube. Peptides were purified using Solaμ plates (Thermo Fisher Scientific), according to the manufacturer's instructions. Purified peptides were analyzed by liquid chromatography-tandem mass spectrometry using an Evosep One LC system (Evosep) coupled to an Eclipse mass spectrometer (Thermo Fisher Scientific). Peptides were separated using the preinstalled 40 Sample-per-Day Whisper method. Chromatographic separation was performed using an Aurora Series Generation 3 15 cm × 75 μm inner diameter, 1.7 μm C18 analytical column (Ion Opticks). Mobile phase A consisted of 0.1% formic acid in water, and mobile phase B contained 0.1% formic acid in 80% acetonitrile. Mass spectrometry data were acquired over 31 minutes in positive ion mode utilizing a data-independent acquisition strategy. MS1 Orbitrap resolution was set to 120,000 within a scan range of 400−1000 m/z, with an AGC target of 300% or 1.2×10^6 and the maximum fill time set to auto. For MS2, Orbitrap resolution was 60,000 with an AGC target of 1000% or 5×10^5 and an auto maximum fill time, within a precursor scan range of 400−1000 m/z and a scan range of 200−1200 m/z. Automatic data-independent acquisition window type was enabled, normalized collision energy was set to 33%, isolation windows were placed at 8 m/z with a window overlap of 1 m/z and optimal window placement enabled. Loop control was enabled and set to 25 number of spectra. FAIMS voltages were set to −50 compensation voltage for both experiments. Raw data were analyzed through Spectronaut's (version 19.7.250203.62635; Biognosys) pulsar search engine, using the reviewed mouse fasta file (UP000000589). Mass spectra were matched using default settings, and peptides were searched, setting the Pulsar search to semispecific and cleavage rules to Trypsin/P and LysC with a maximum and minimum peptide length of 48 and 6 amino acids. No imputation was performed, and the MS1 area of proteotypic peptides was considered for quantification.

In vitro digestion of human dermokine by human meprin α

As described, HEK293T cells were transfected with a plasmid encoding C-terminally FLAG-tagged human dermokine isoform beta (UniProt identification: Q6E0U4-1). Cell culture supernatant was collected after overnight incubation in fetal calf serum–free DMEM medium and ultracentrifuged (2 hours, 186,000g, 4 °C) to remove cell debris and micro vesicles. Recombinant N-terminally Strep-tagged human meprin α was generated by transient transfection of HEK293T cells. Culture supernatants were concentrated with a 10-kDA MWCO Amicon column (Merck) and purified with Strep-tactin resin gravity flow columns at 4 °C. After elution, buffer was exchanged to 20 mM HEPES pH 7.0, and protein concentration was determined by photometry. Activation of recombinant human meprin α was achieved by incubation with bovine trypsin (10 μg/μl) for 20 minutes at 37 °C. Afterward, trypsin was inhibited by addition of ovomucoid (25 μg/μl) and incubation for 10 minutes at 37 °C. Cell culture supernatant containing human dermokine was incubated with 1 nM activated recombinant human meprin α for up to 24 hours. For subsequent western blot analysis, proteins were precipitated from the supernatant with trichloroacetic acid.

SUPPLEMENTARY REFERENCES

Jaskolski F, Mulle C, Manzoni OJ. An automated method to quantify and visualize colocalized fluorescent signals. J Neurosci Methods 2005;146:42–9.

Leclerc EA, Huchenq A, Kezic S, Serre G, Jonca N. Mice deficient for the epidermal dermokine β and γ isoforms display transient cornification defects. J Cell Sci 2014;127:2862–72.

Peters F, Scharfenberg F, Colmorgen C, Armbrust F, Wichert R, Arnold P, et al. Tethering soluble meprin α in an enzyme complex to the cell surface affects IBD-associated genes. FASEB J 2019;33:7490–504.

Kalogeropoulos K, Moldt Haack A, Madzharova E, Di Lorenzo A, Hanna R, Schoof EM, et al. CLIPPER 2.0: peptide-level annotation and data analysis for positional proteomics. Mol Cell Proteomics 2024;23:100781.

Meyer B, Chiaravalli J, Gellenoncourt S, Brownridge P, Bryne DP, Daly LA, et al. Characterising proteolysis during SARS-CoV-2 infection identifies viral cleavage sites and cellular targets with therapeutic potential. Nat Commun 2021;12:5553.

Pettitt SJ, Liang Q, Rairdan XY, Moran JL, Prosser HM, Beier DR, et al. Agouti C57BL/6N embryonic stem cells for mouse genetic resources. Nat Methods 2009;6:493–5.

Poueymirou WT, Auerbach W, Frendewey D, Hickey JF, Escaravage JM, Esau L, et al. F0 generation mice fully derived from gene-targeted embryonic stem cells allowing immediate phenotypic analyses. Nat Biotechnol 2007;25:91–9.

Van Keymeulen A, Rocha AS, Ousset M, Beck B, Bouvencourt G, Rock J, et al. Distinct stem cells contribute to mammary gland development and maintenance. Nature 2011;479:189–93.

Walter K, Ziesche F. Apparatus and method, particularly for microscopes and endoscopes, using baseline estimation and half-quadratic minimization for the deblurring of images. European Patent Office 2019;479. WO 2019/185174 A1.

Weng SSH, Demir F, Ergin EK, Dirnberger S, Uzozie A, Tuscher D, et al. Sensitive determination of proteolytic proteoforms in limited microscale proteome samples. Mol Cell Proteomics 2019;18:2335–47.

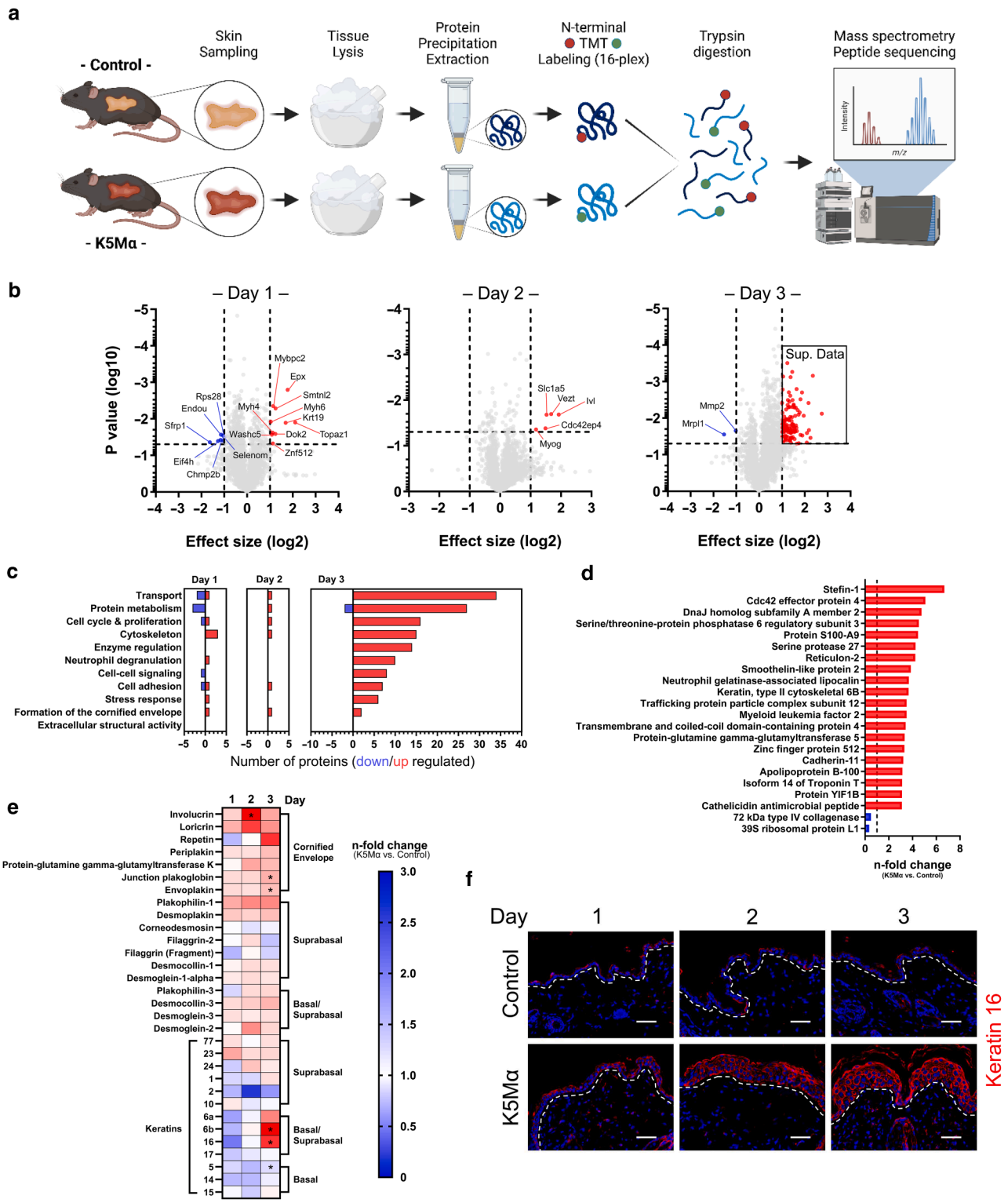

Supplementary Figure S1. Alterations in the skin proteome of K5Mα mice. **(a)** Schematic illustration of the sample preparation work flow for mass spectrometry–based global proteome analysis. Skin samples from control (n = 3) and K5Mα (n = 3) mice were excised after killing on days 1–3 after topical treatment with TAM, pulverized in a liquid nitrogen–cooled mortar, and proteins isolated by methanol/chloroform precipitation. Proteins were TMT labeled, trypsin digested, and subjected to LC-MS/MS analysis. **(b)** Volcano plots display all detected proteins by LC-MS/MS analysis in skin samples of K5Mα mice compared with those of control mice on day 1, 2, and 3 after TAM treatment. Dashed lines (- - -) mark 0.5- and 2.0-fold changes in effect size (x-axis; log2 transformed) and a $P = .05$ (y-axis; log10 transformed), the threshold for statistical significance. Proteins significantly higher (effect size ≥2.0-fold; red dots) or lower (effect size ≤0.5-fold; blue dots) abundant in the skin of K5Mα compared with those of control mice are highlighted. **(c)** Bar charts display the number of significantly higher (red bars) and lower (blue bars) abundant proteins detected by LC-MS/MS in the skin of K5Mα compared with that of control mice on day 1, 2, and 3 after TAM treatment grouped by gene ontology annotations. **(d)** Bar chart displays n-fold changes (sorted by highest to lowest) in the levels of significantly ($P < .05$, 2-tailed unpaired *t*-test) higher (red bars; ≥2.0-fold) and lower (blue bars; ≤0.5-fold) abundant proteins detected by LC-MS/MS in the skin

of K5Mα compared with that of control mice on day 3 (only top 20 higher abundant proteins) after topical treatment with TAM. **(e)** Heatmap displays mean n-fold changes in the level of proteins associated with keratinocyte differentiation status detected by LC-MS/MS in the skin of K5Mα mice compared with that of control mice on day 1, 2, and 3 after TAM treatment. Proteins higher (red) and lower (blue) abundant in the skin of K5Mα than in that of control mice are highlighted by color gradients. Statistically significant differences ($P < .05$, annotated by an asterisk *) were tested by 2-tailed unpaired *t*-test prior to data normalization using signal intensities measured by LC-MS/MS. **(f)** Representative immunofluorescence images of skin sections from control (n = 3) and K5Mα (n = 3) mice on day 1−3 after topical TAM treatment. Keratin 16 (red) was detected by indirect immunofluorescence staining. Nuclei were stained with DAPI. Bars = 50 μm. Graphical illustration in **a** was created with BioRender.com. LC-MS/MS, liquid chromatography-tandem mass spectrometry; TAM, 4-hydroxytamoxifen.

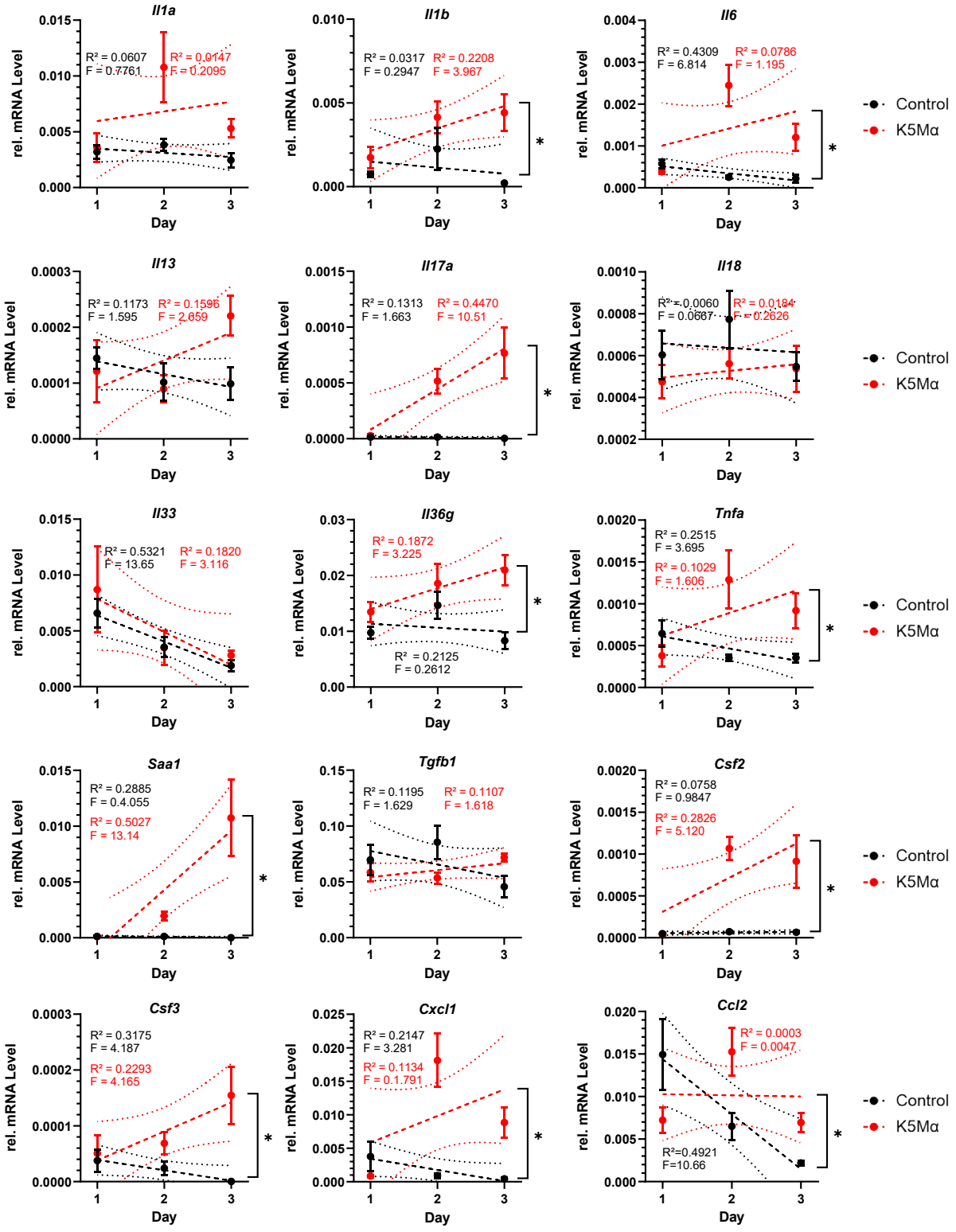

Supplementary Figure S2. Expression levels of cytokines and chemokines in the skin of control and K5Mα mice. Relative mRNA levels of *Il1a*, *Il1b*, *Il6*, *Il13*, *Il17a*, *Il18*, *Il33*, *Il36g*, *Tnfa*, *Saa1*, *Tgfb1*, *Csf2*, *Csf3*, *Cxcl1*, and *Ccl2* in skin samples from control (n = 5 per day) and K5Mα (n = 5 per day) mice at days 1−3 after TAM treatment. mRNA levels were normalized to *Gapdh* mRNA levels in the respective sample by $2^{-\Delta\Delta Ct}$ method. Data points and error bars display mean values ± SEM. Results from linear regression (dashed lines) and respective 95% confidence band of the best-fit line (dotted lines) are displayed. Slopes (s) and elevations (e) were tested for significant differences (*Il1a*[s]: F = 0.3831, *P* = .5413; *Il1b*[e]: F = 9.075, *P* = .0060; *Il6*[e]: F = 8.839, *P* = .0066; *Il13*[s]: F = 4.044, *P* = .0548; *Il17a*[s]: F = 9.989, *P* = .0042; *Il18*[s]: F = 0.2757, *P* = .6042; *Il33*[s]: F = 0.1064, *P* = .7469; *Il36g*[e]: F = 10.86, *P* = .0028; *Tnfa*[e]: F = 4.269, *P* = .0489; *Saa1*[s]: F = 10.56, *P* = .0035; *Tgfb1*[s]: F = 2.917, *P* = .1000; *Csf2*[s]: F = 4.977, *P* = .0349; *Csf3*[s]: F = 5.269, *P* = .0312; *Cxcl1*[e]: F = 8.695, *P* = .0065; *Ccl2*[s]: F = 4.974, *P* = .0349). Statistically significant differences (*P* < .05) are indicated by an asterisk (*). TAM, 4-hydroxytamoxifen.

Supplementary Figure S3. Filtering TAILS data for meprin α–specific cleavage criteria identified 10 potential substrates. Filtering steps (blue boxes) and exclusion criteria (red boxes) as well as illustration of the stepwise filtering process for identification of peptides within the TAILS dataset potentially generated by meprin α cleavage.

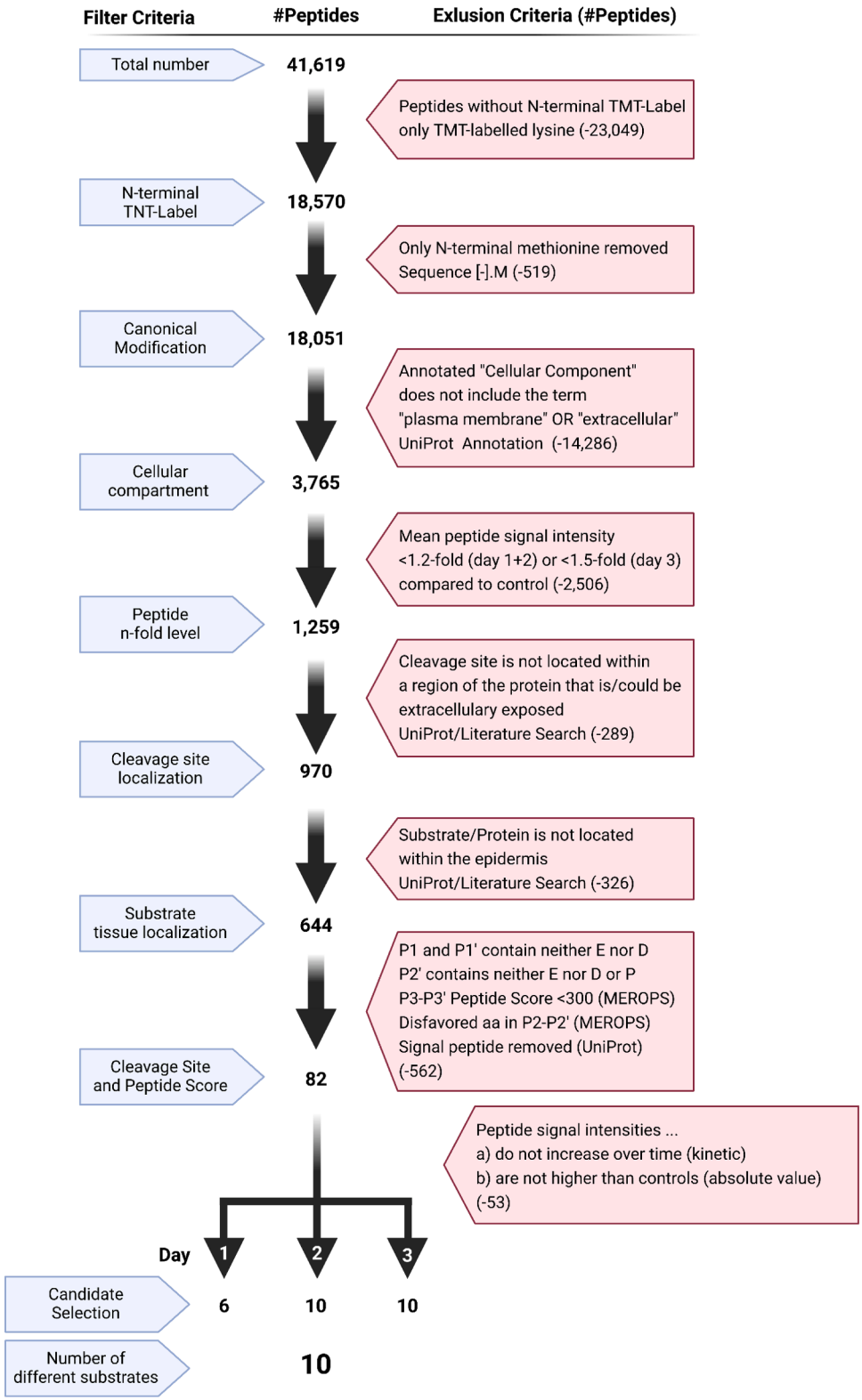

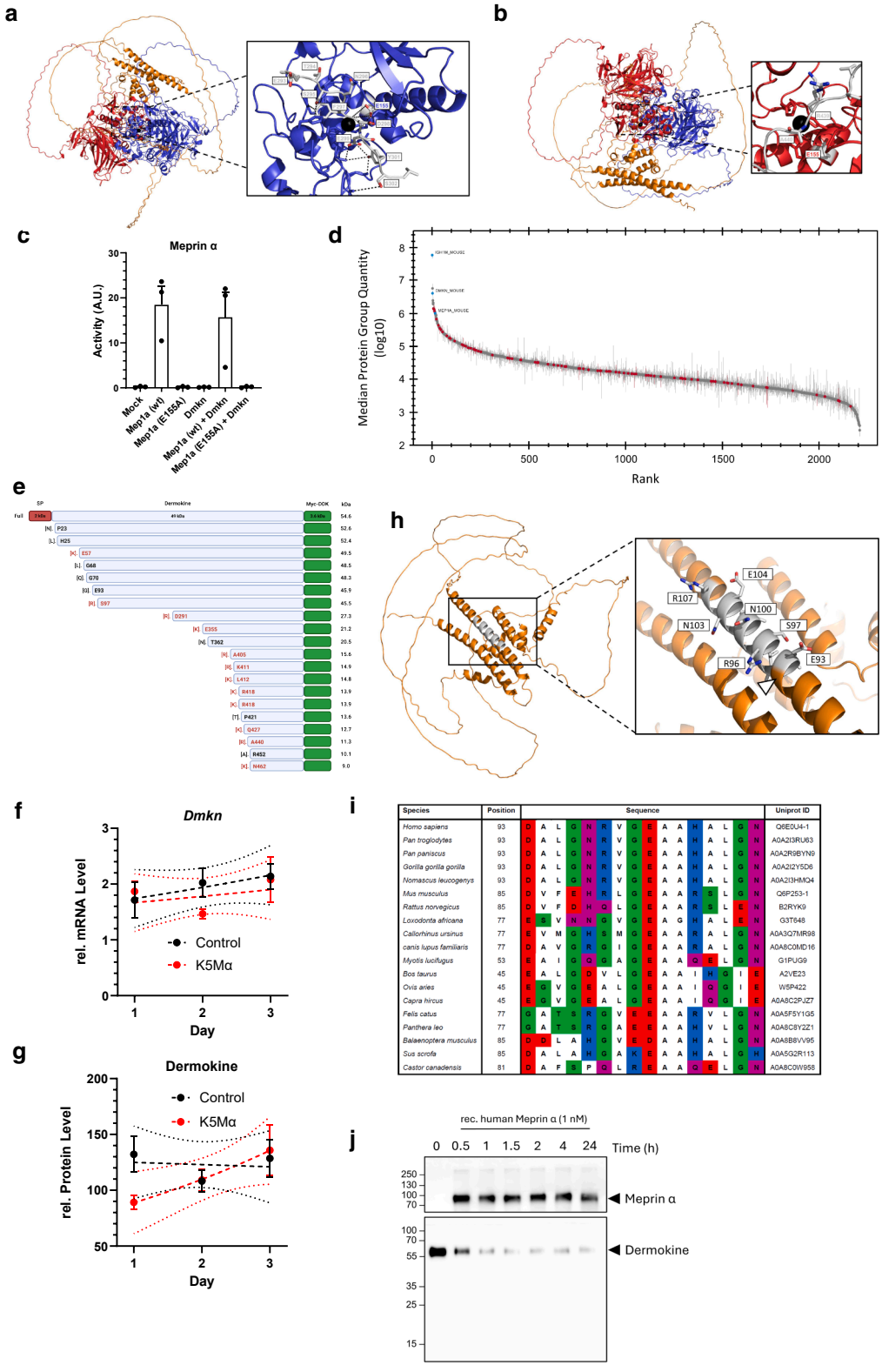

Supplementary Figure S4. Structural modeling of dermokine in complex with meprin α and cleavage site conservation. **(a, b)** AlphaFold 3 model of murine dermokine β (UniProt ID: Q6P253-1, without N-terminal signal peptide sequence) in complex with the homodimeric ectodomain of murine meprin α (P28825, without N-terminal signal and propeptide sequences [N65 to M713]). Dermokine (orange) and meprin α subunits (red and blue) are presented as ribbon diagrams. Zoom-ins show the orientation and interaction of dermokine in the active site of meprin α. Side chains of dermokine are color coded by elements (carbon [gray], oxygen [red], and nitrogen [blue]), and amino acids in 1-letter code as well as respective position are annotated (gray). Side chain of the catalytic glutamate (E155) within the active site of meprin α is also presented, color coded, and annotated ([**a**] blue or [**b**] red). Zinc ion is presented as black sphere. Predicted noncovalent interactions between dermokine and meprin α are highlighted by dashed lines (- - -): **(a)** Hydrogen bonds between S295-H155, D298-C127, E299-H212, Y301-G239, Y301-H212, Y301-L210, and S302-F216. Binding of dermokine F297 into a pocket formed by meprin α F163 and I131 is

Supplementary Table S1. Antibodies

Target (Conjugate) [Clone]	Host [Isotype]	Concentration/Dilution (Application)	Manufacturer (Catalog ID)
Meprin α anti-serum [custom generated]	Rabbit	1:5000 (WB) 10 µl/800 µg protein (IP)	Pineda Antibody Service
Ki-67 [D3B5]	Rabbit [IgG]	1:200 (IF)	Cell Signaling Technology (112202)
Meprin α [polyclonal]	Goat	1 µg/ml (IF)	Bio-Techne (AF4007)
Cytokeratin 16 [polyclonal]	Rabbit	1 µg/ml (IF)	Proteintech (17265-1-AP)
S100A9 [D3U8M]	Rabbit [IgG]	1:200 (IF)	Cell Signaling Technology (73425)
CD45 [30-F11]	Rat [IgG_{2b}]	1 µg/ml (IF)	Santa Cruz Biotechnology (sc-53665)
Rabbit IgG H+L (HRP) [polyclonal]	Goat	1:5000 (WB)	Jackson ImmunoResearch (111-035-003)
Mouse IgG H+L (HRP) [polyclonal]	Sheep	1:5000 (WB)	Jackson ImmunoResearch (515-035-003)
Goat IgG H+L (AlexaFluor488) [polyclonal]	Donkey	2 µg/ml (IF)	Thermo Fisher Scientific (A-11055)
Rabbit IgG H+L (AlexaFluor647) [polyclonal]	Donkey	2 µg/ml (IF)	Thermo Fisher Scientific (A-31573)
Gapdh [14C10]	Rabbit [IgG]	1:5000 (WB)	Cell Signaling Technology (2118)
FLAG-Tag [M2]	Mouse [IgG_1]	1:1000 (WB) 1 µg/800 µg protein (IP)	Merck (F3165)
Dermokine [polyclonal]	Rabbit [IgG]	2 µg/ml (IF)	Proteintech (16252-1-AP)
Dermokine [custom generated] (Leclerc et al, 2014)	Rabbit [IgG]	1:500 (IF) 1:1000 (WB)	Genosphere
Myc-Tag [9B11]	Mouse [IgG_{2a}, κ]	1:2500 (WB)	Cell Signaling Technology (2276)

Abbreviations: HRP, horse radish peroxidase; ID, identification; IF, immunofluorescence; IP, immunoprecipitation; WB, western blot.

shown. Distance of meprin α E155 side chain to the dermokine peptide bonds between F297-D298 and D298-E299 is shown. **(b)** Distance of meprin α E155 side chain to the dermokine peptide bond between R439 and A440. **(c)** Meprin α activity in the culture supernatant of HEK293T cells transiently transfected with an empty control plasmid (Mock) or plasmids encoding wildtype (WT) murine meprin α (*Mep1a*), C-terminally Myc-FLAG–tagged murine dermokine (*Dmkn*), and/or a catalytically inactive meprin α variant (*Mep1a* [E155A]). Activity is plotted in A.U. Bar charts and error bars display mean ± SEM (n = 3 per group). **(d)** Median quantity of proteins detected by mass spectrometry in lysates of HEK293T cells transiently transfected with plasmids encoding *Mep1a* WT and *Dmkn* after co-IP of dermokine. Proteins are grouped and ranked according to their abundance. Highlighted are murine Ig-gamma chain C region (IGH1M_MOUSE; antibody used for co-IP), murine dermokine (DMKN_MOUSE), and murine meprin α (MEP1A_MOUSE). **(e)** Schematic illustration of the full-length C-terminally Myc-FLAG (Myc-DDK)–tagged murine dermokine (*Dmkn*) encoded in the plasmid used for overexpression as well as putative CTFs corresponding to the dermokine-derived peptides identified by mass spectrometry after co-IP. Annotated are the SP, the N-terminal amino acids in 1-letter codes, including position in the protein and the putative size of full-length dermokine, and CTFs in kDa. Amino acids in squared brackets are annotated on the basis of the protein sequence obtained from UniProt database. Cleavage sites marked in red are potentially generated by trypsin digestion during sample preparation. **(f)** Relative mRNA levels of *Dmkn* in skin samples from control (n = 5 per day) and K5Mα (n = 5 per day) mice at days 1–3 after TAM treatment. *Dmkn* levels were normalized to *Gapdh* levels in the respective sample by $2^{-\Delta\Delta Ct}$ method. Data points and error bars display mean values ± SEMs. Results from linear regression (dashed lines) and respective 95% confidence band of the best-fit line (dotted lines) are displayed. **(g)** Relative dermokine protein levels detected by LC-MS/MS in skin samples from control (n = 3 per day) and K5Mα (n = 3 per day) mice at days 1–3 after TAM treatment. Data points and error bars display mean values ± SEM. Results from simple linear regression (dashed lines) and respective 95% confidence band of the best-fit line (dotted lines) are displayed. **(h)** AlphaFold 3 model of murine dermokine β (UniProt ID: Q6P253-1, without N-terminal signal peptide sequence) presented as ribbon diagram. Zoom-in highlights the cleavage site by meprin α (Δ) as well as the peptide identified by mass spectrometry after co-IP. Side chains of the peptide are color coded by elements (carbon [gray], oxygen [red], and nitrogen [blue]), and amino acids in 1-letter code as well as respective position are annotated. **(i)** Alignment of the protein sequences around the identified cleavage site in dermokine from various mammalian species. Amino acids were color coded according to their chemical properties: polar (green/violet), basic (blue), acidic (red), and hydrophobic (white). **(j)** Changes in the levels of human dermokine after incubation with active recombinant human meprin α (1 nM) for up to 24 hours. Both dermokine and meprin α were generated by transient transfection of HEK293T cells with plasmids encoding *DMKN* or *MEP1A*. Graphical illustration in **e** was created with BioRender.com. A.U., arbitrary unit; co-IP, coimmunoprecipitation; CTF, C-terminal fragment; HEK293T, human embryonic kidney 293T; ID, identification; LC-MS/MS, liquid chromatography-tandem mass spectrometry; SP, signal peptide; TAM, 4-hydroxytamoxifen; WT, wild-type.

Supplementary Table S2. Primer

Gene	Transcript ID	Sequence (5′−3′)	Amplicon (bp)	T_m (°C)
S100a8	NM_013650.2	fw: GTCCTCAGTTTGTGCAGAATATAAA rev: GCCAGAAGCTCTGCTACTCC	159	80.95
S100a9	NM_001281852.1	fw: CCCTGAGCAAGAAGGAATTCAG rev: GGCTTCATTTCTCTTCTCTTTCTTC	80	77.68
Saa1	NM_009117.4	fw: CCAGGAGACACCAGGATGAAG rev: CCCTTGGAAAGCCTCGTGA	108	82.63
Il1a	NM_010554.4	fw: CGTGTTGCTGAAGGAGTTGC rev: CTGTCATAGAGGGCAGTCCC	185	82.48
Il1b	NM_008361.4	fw: TGCCACCTTTTGACAGTGATG rev: CAAAGGTTTGGAAGCAGCCC	84	80.01
Il6	NM_031168.2	fw: GCCTTCTTGGGACTGATGCT rev: TGCCATTGCACAACTCTTTTC	181	82.68
Il13	NM_008355.3	fw: CACACAAGACCAGACTCCCCT rev: GCCATGCAATATCCTCTGGGT	145	85.04
Il17a	NM_010552.3	fw: TGGACTCTCCACCGCAATG rev: TTTCCCTCCGCATTGACACA	95	82.94
Il18	NM_008360.2	fw: TACAAGCATCCAGGCACAGC rev: CTGATGCTGGAGGTTGCAGA	122	85.56
Il33	NM_001164724.2	fw: GGGCTCACTGCAGGAAAGT rev: TGGTCTTCTGTTGGGATCTTCTT	183	83.02
Il36g	NM_153511.3	fw: ACTTTGCTGCTAAAGGAAGAGAA rev: CCGGGTGTGGTAAAACAGGA	84	79.40
Tnfa	NM_013693.3	fw: TAGCCCACGTCGTAGCAAAC rev: GCAGCCTTGTCCCTTGAAGA	170	86.75
Csf3	NM_009971.1	fw: CATGAAGCTAATGGCCCTGC rev: CTGACAGTGACCAGGGGAAC	84	83.87
Csf2	NM_009969.4	fw: CTAAGGTCCTGAGGAGGATGTG rev: ACGACTTCTACCTCTTCATTCAAC	187	85.05
Cxcl1	NM_008176.3	fw: CCCAAACCGAAGTCATAGCCA rev: CCAGACAGGTGCCATCAGAG	153	83.06
Ccl2	NM_011333.3	fw: CACTCACCTGCTGCTACTCA rev: GCTTGGTGACAAAAACTACAGC	117	81.97
Tgfb1	NM_011577.2	fw: GCTGAACCAAGGAGACGGAA rev: ATGTCATGGATGGTGCCCAG	138	84.21
Dmkn	NM_172899.4	fw: TGGAAACAGATTGAGGGTTCAG rev: CCTTGGCAGTGGTCTTGGTAT	181	81.89
Gapdh	NM_001289726.2	fw: GGAAGGGCTCATGACCACAGT rev: ATCACGCCACAGCTTTCCAG	82	83.57

Abbreviations: fw, forward; ID, identification; rev, reverse.

Supplementary Table S3. Meprin α–Preferred Amino Acids at Positions P3 to P3′

Amino Acid/Position	P3	P2	P1	P1′	P2′	P3′
G	57	35	77	43	67	93
P	65	47	4	1	129	101
A	54	76	94	79	61	42
V	58	73	5	47	62	68
L	59	96	43	50	50	62
I	45	41	3	25	30	52
M	16	20	23	15	15	13
F	30	41	43	25	19	18
Y	14	32	25	17	17	13
W	5	8	15	1	11	3
S	43	45	75	55	47	33
T	37	35	8	64	33	52
C	2	7	3	2	2	5
N	23	22	55	16	15	19
Q	36	73	50	12	37	24
D	23	22	74	201	45	31
E	32	44	86	91	83	72
K	87	26	17	9	32	49
R	62	9	41	11	10	10
H	20	23	35	12	11	13

Data obtained from the MEROPS database.

Supplementary Table S4. Amino Acids Sequences of Meprin α and Dermokine Used for AlphaFold 3 Modeling

Protein (UniProt ID)	Sequence (N- to C-Terminus)
Meprin α subunit alpha (P28825)	NAMRDPSSRWKLPIPYILADNLELNAKGAILHAFEMFRLKSCVDFKPYEGESSYIIFQKLS GCWSMIGDQQVGQNISIGEGCDFKATIEHEILHALGFFHEQSRTDRDDYVNIWWDQIITD YEHNFNTYDDNTITDLNTPYDYESLMHYGPFSFNKNESIPTITTKIPEFNTIIGQLPDFSAIDLIRLNR MYNCTATHTLLDHCDFEKTNVCGMIQGTRDDADWAHGDSSQPEQVDHTLVGQCKGAGYFMFF NTSLGARGEAALLESRILYPKRKQQCLQFFYKMTGSPADRFEVWVRRDDNAGKVRQLAKIQTF QGDSDHNWKIAHVTLNEEKKFRYVFLGTKGDPGNSSGGIYLDDITLTETPCPAGVWTIRNISQI LENTVKGDKLVSPRFYNSEGYGVGVTLYPNGRITSNSGFLGLTFHLYSGDNDAILEWPVENRQAIMTILDQ EADTRNRMSLTLMFTTSKNQTSSAINGSVIWDRPSKVGVYDKDCDCFRSLDWGWGQA ISHQLLKRRNFLKGDSLIIFVDFKDLTHLNRTEVPASARSTMPRGLLLQGQESPALGESSRKAMLEES LPSSLGQRHPSRQKRSVENTGPMEDHNWPQYFRDPCDPNPCQNEGTCVNVKGMASCRCVS GHAFFYAGERCQAM
Dermokine (Q6P253-1)	NPLHSGGEGTGASAAHGAGDAISHGIGEAVGQGAKEAASSGIQNALGQGHG EEGGSTLMGSRGDVFEHRLGEAARSLGNAGNEIGRQAEDIIRQGVDAVHNAGS WGTSGGHGAYGSQGGAGVQGNPGPQGTPWASGGNYGTNSLGGSVGQGG NGGPLDYETNAQGAVAQPGYGTVRGNNQNSGCTNPPPSGSHESFSNSGGSS NDGSRGSQGSHGSNGQGSSGRGGGQGNSDNNGSSSSSSGSNSGNSNSGN SGNSNSGNSGNSGSGSRDIETSNFDEGYSVSRGTGSRGGSGGSGGSGGS GGSGGSGGGNKPECNNPGNDVRMAGGSGSQGHGSNGGNIQKEAVNG LNTMNSDASTLPFNIDNFWENLKSKTRFINWDAINKGHAPSPSTR ALLYFRKLWENFKRSTPFFNWKQIEGSDLSSLQKRAGGADQFSK PEARQDLSADSSKNYYNNQQVNPTYNWQYYTKTTA KAGVTPSSSSASRAQPGLLKWLKFW

Abbreviation: ID, identification.